Title
Knottins are a new family of secreted virulence factors that are required for the virulence of the intracellular fungal pathogen Histoplasma capsulatum

Author
Rodriguez, Rosa Angelica

Publication Date
2023

Peer reviewed|Thesis/dissertation

Knottins are a new family of secreted virulence factors that are required for the virulence of the intracellular fungal pathogen Histoplasma capsulatum

by

Rosa Angelica Rodriguez

DISSERTATION

Submitted in partial satisfaction of the requirements for degree of

DOCTOR OF PHILOSOPHY

in

Genetics

in the

GRADUATE DIVISION

of the

UNIVERSITY OF CALIFORNIA, SAN FRANCISCO

Approved:

DocuSigned by:
Shaeri Mukherjee
7AA908684B40471...

Shaeri Mukherjee

Chair

DocuSigned by:
Joanne Engel

Joanne Engel

DocuSigned by:
Anita Sil
...459...

Anita Sil

DocuSigned by:
David Toczyski
402B6252FD6D45E...

David Toczyski

Committee Members

This dissertation is dedicated to my parents, Oscar and Rosalba. Without your love, support and sacrifices I would not be where I am today. I owe my success to you. Sin su amor, apoyo y sacrificios no estaría donde estoy hoy. A ustedes les debo mi exito. This dissertation is also dedicated to Donald Warren for always being my rock and keeping me sane.

Acknowledgements

Many people were involved to make this work possible. First, I would like to thank Anita Sil, my PhD advisor, for providing such a welcoming and supportive environment in which to do amazing biology. Her kindness, support, and mentorship have helped me grow into the scientist I am today. Thank you for always encouraging me to continue even when things got tough. I would also like to thank the member of the thesis committee, Shaeri Mukherjee, David Toczyski and Joanne Engel for the invaluable suggestions and discussion throughout my time at UCSF.

I couldn't continue without thanking members of the Sil lab both past and present. Past members like Bevin English, Lauren Rodriguez, and Allison Cohen all made coming to lab actually fun. The conversations we had in the tiny breakroom are things I will always remember. You weren't just lab mates, you became friends. Shout out to current members, Anna, Nebat, Dror, Sarah, Christina, Janey, Murat, and Anyce for being real ones and taking on such challenging but exciting projects. I'm excited to see where things go. A special shoutout to Janey and Bevin, the BSL3 czar, for all their help with the mouse infections. An extra special thanks to Bevin for babysitting me in the BSL3 while I counted almost 1000 plates. I can never give you back that time, but we did listen to some awesome jams.

None of this work would have been possible without my lab twin, Dinara. We started at the same time in the lab. I cannot begin to thank you for all you did. I could always turn to you and ask the silly questions without judgement. We took every step of graduate school together and without you next to me this time would have been impossible. You have become one of my closest friends.

I would be remiss if I didn't thank David Weisblat. When I started my undergrad, I don't think I really knew what research was. David gave me first chance to work in a lab even before I had taken general biology. I knew nothing but he was willing to teach me. I will forever be in debt to you for showing me how fun and exciting it could be to be a scientist plus working with leeches is always a fun tidbit to say. I would also like to thank the Biology Scholars program at UC Berkeley. Without their guidance and financial support, I would have never been able to afford to have the research experiences I had in undergrad.

Next, I must thank the Tetrad graduate program because without it I would not have met someone who has become one of my best friends. Paola Andrea Soto Perez is someone who I have had the fortune to have met. She is the single most grounded person I have had the privilege to make my acquaintance. She will never sugar coat something and I know I can count on her for real talk. Over the years there is no one who expresses her inside thoughts like her and it's a breath of fresh air. Thanks friend!

I have saved the best for last. I would without a doubt not be where I am today without Donald Warren. We met in freshman year of high school and have been the best of friends since. His understanding but willingness to bring me back to reality has always been so important to me. He is the one person whose opinion always matters. I have always counted on his support, and I am deeply grateful for it. This accomplishment is as much mine as it is yours.

Lastly, I must thank my parents, Oscar and Rosalba. They have sacrificed everything for me. They understood the value of education even though they never were given the opportunity. Without their sacrifice I would not have the privilege to pursue this

degree. Thank you for your support, love and understanding. I am blessed to have you in my life and love you unconditionally. Everything I have done is as much for you as it for me.

Por último, debo agradecer a mis padres. Lo han sacrificado todo por mí. Entendieron el valor de la educación a pesar de que nunca se les dio la oportunidad. Sin su sacrificio no tendría el privilegio de obtener este título. Todo lo que he hecho hasta este momento ha sido por nosotros. Gracias por su apoyo, amor y comprensión. Tengo la suerte de tener los en mi vida y amar los incondicionalmente. Todo lo que he hecho es tanto para ustedes como para mí.

Contributions:

Some data and text in Chapter 2 is reprinted from the following article:

Gilmore, S.A., et al., *Genome-Wide Reprogramming of Transcript Architecture by Temperature Specifies the Developmental States of the Human Pathogen Histoplasma.* PLoS Genet, 2015. **11**(7): p. e1005395.

Some data and text in Chapter 2 and 3 are reprinted from the following dissertation: Azimova, D. (2021). *Histoplasma capsulatum* secretes cysteine-rich protein virulence factors to lyse host macrophages. *UCSF*. ProQuest ID: Azimova_ucsf_0034D_12196. Merritt ID: ark:/13030/m5t78jtn. Retrieved from https://escholarship.org/uc/item/8ms2408n

The some of the data presented in this dissertation has been prepared for the following manuscript:

Rodriguez, RA.*, Azimova, D.*, Voorhies, M., English, BC., Symington, JW., Gilmore, S., and Sil, A. Knottins are a new family of secreted virulence factors that are required for the virulence of the intracellular fungal pathogen *Histoplasma capsulatum*. Manuscript in preparation.

I (Rosa Rodriguez), conceived, designed, and executed the experiments that were essential for this work. I collected and analyzed the data and wrote this dissertation. This work was accomplished under the direct guidance and financial support of Dr. Anita Sil.

Knottins are a new family of secreted virulence factors that are required for the virulence of the intracellular fungal pathogen *Histoplasma capsulatum*

Rosa Rodriguez

Abstract

Intracellular pathogens have developed strategies like secreting virulence factors to aid in replication and survival. *Histoplasma capsulatum* (*Hc*) is a thermally dimorphic human fungal pathogen that causes apoptosis of macrophages through the induction of the Integrated Stress Response (ISR). The mechanisms through which *Hc* induces host cell death are still poorly understood. In this work, we take a bioinformatic and genetic approach to identify and study novel *Hc* effectors. Known fungal effectors tend to be highly expressed in the pathogenic form of the organism, small, secreted, and cysteine-rich. Using these criteria, we identified many putative *Hc* effectors, some of which contained homology to the cysteine knot gene family called knottins. Knottins contain a 6-cysteine motif that creates three disulfide bridges forming a stable knot structure. We wrote a naïve algorithm to mine the *Hc* genome for knottins and identified a total of 26 putative knottins. Furthermore, we observed a unique and massive expansion of putative knottin genes in all *Histoplasma* species that was not observed across the fungal kingdom. We characterized four knottins named *KNOT1*, *KNOT2*, *KNOT3* and *KNOT4* and discovered that all four proteins localize to the host cytosol during *Hc* infection of macrophages. Using CRISPR-Cas9, we generated deletion mutants and discovered that *KNOT1*, *KNOT2* and *KNOT4* are dispensable for *in vitro* growth. Surprisingly, deletion of *KNOT3* resulted in a moderate growth defect. We observed that *KNOT1*, *KNOT3,* and *KNOT4* were all

required for optimal *Hc* intracellular growth within macrophages as well as macrophage lysis. In contrast, *KNOT2* was required for macrophage lysis but was dispensable for intracellular growth. Intriguingly, these knottins proteins were not required to stimulate a host pathway, the Integrated Stress Response (ISR), which was previously shown to be required for optimal macrophage lysis. Instead, we observe no difference in ISR induction in the absence of these knottins, suggesting that they interact with other host cellular pathways that are required for lysis. Of these four knottins, we chose to characterize *KNOT2* and *KNOT4* in the mouse model of infection. Mice failed to succumb to infection with mutant *Hc* strains lacking *KNOT2 or KNOT4.* Interestingly, the *knot4Δ* mutant displays a modest decrease in fungal burden in the mouse, whereas the *knot2Δ* mutant is able to grow to wild-type levels. These data indicate that *KNOT2* and *KNOT4* are dispensable for fungal burden and may instead manipulate other host processes such as the immune response. Taken together, this work identifies a new family of virulence factors and highlights how *Hc* is using a varied arsenal of effectors to cause disease.

Table of Contents

List of figures:

List of Tables

Chapter 1: Background

Intracellular pathogens

Intracellular pathogens have evolved a multitude of strategies to avoid detection and survive within their hosts[1]. For example, within the host, intracellular pathogens must escape the phagosomal compartment or alter it in a way that avoids fusion and degradation by the lysosome[2, 3]. One common strategy to create a replicative niche and/or manipulate host cell biology to benefit the needs of the pathogen is the use of secreted effectors[4].

There are many examples in the literature of intracellular pathogens like *Mycobacterium tuberculosis*[5-7], *Listeria monocytogenes*[8, 9], and *Legionella pneumophila*[10, 11] that use secreted effectors to cause disease. Unique to bacterial pathogens is the use of specialized secretion systems to deliver diverse molecules to aid in pathogenesis. These needle-like machines can puncture the host membranes and directly insert microbial effectors into host cells. These effectors can contribute to pathogenesis by acting as toxins or interacting with host proteins to affect cellular pathways[12]. The paradigms for how secreted effectors are delivered and function come in large part from bacterial pathogens[13].

In eukaryotic pathogens, many of the examples of secreted effectors come from plant fungal pathogens. Due in part to their agricultural relevance, a handful of effectors have been identified in fungi like *Ustilago maydis*[14], *Magnoporthe oryzae*[15] or *Cladosporium fulvum*[16, 17]. However, in human fungal pathogens we have a far more limited understanding of effectors that aid the pathogen in causing disease. The best-known example is in *Candida albicans* where hyphae secrete Candidalysin[18], a peptide

that permeabilizes the host cell membrane, leading to host cell death. In *Histoplasma capsulatum (Hc),* we have a very limited understanding of fungal effectors that promote pathogenesis. Identifying new virulence factors in human fungal pathogens can help us understand how these fungi cause disease in their hosts. We can use preexisting paradigms to identify novel mechanisms through which *Hc* manipulates its environment.

Phytopathogenic fungi

Approximately, 8000 species of fungi are associated with infection of plants, destroying upwards of 30% of crops annually[19-21]. Plant fungal pathogens use a variety of effector molecules to cause disease. These effectors have been shown to aid the pathogen in penetrating host cell membranes, nutrient acquisition, and avoiding detection by the host immune system[22]. Studies of known effectors reveal common features that could be used to identify putative effectors in other organisms. Plant pathogen effectors tend to be small (less than 300 amino acids), secreted, and have a high cysteine content. Cysteines form disulfide bridges which can promote stable folding of pathogen effectors, even in highly reducing environments like the host cell cytosol. Effectors also tend to be highly expressed in the infectious form of the fungus. Lastly, effectors tend to have no predicted Pfam domains, generally making them proteins of unknown function. We applied these guidelines to the *Hc* genome to identify putative effectors.

Hc epidemiology and pathogenesis

The quest to identify *Hc* effectors is driven by biological interest as well as disease impact. *Hc* is the causative agent of histoplasmosis. In immunocompetent individuals, exposure to this fungus often remains unnoticed or manifests as flu-like respiratory symptoms, whereas immunocompromised individuals can develop life-threatening

disseminated infections[23-26]. *Hc* is found worldwide but within the United States is endemic to the Ohio and Mississippi River Valleys although cases have been reported across the country[23, 27, 28].

Hc is a thermally dimorphic fungus[29]. The infectious form of *Hc* grows in the soil as a multicellular saprophytic mold (the hyphal form) that produces spores called conidia. Two types of conidia are found in the soil; macroconidia that are between 8-15 μm and microconidia that are between 2-5 μm[24]. Upon soil disruption, fragments of the mold and spores are aerosolized and are readily inhaled by mammalian hosts. Once inside the lungs, the temperature increase from ambient temperature to body temperature (37°C) is sufficient to induce a morphological transition from the soil form to the host form, the unicellular budding yeast. Published work from our lab has shown that *Hc* hyphae and yeast display distinct expression profiles, giving *Hc* the tools necessary for survival in different environmental conditions[30].

Hc yeast are readily phagocytosed by resident immune cells like alveolar macrophages[31, 32]. Inside the host macrophage, *Hc* replicates intracellularly in a specialized compartment called the phagosome[33, 34]. We know that *Hc* actively prevents phagosome maturation and acidification by blocking fusion of the phagosome to the lysosome[35-37]. These manipulations allow *Hc* to replicate intracellularly, ultimately leading to lysis of the host cell and reinfection of neighboring cells.

Hc virulence factors

There are a handful of previously identified *Hc* virulence factors that are necessary for intracellular survival or immune evasion. These virulence factors tend to be highly expressed in the yeast form of *Hc*[30]. The *Hc* yeast transcription program is regulated by

a network of temperature responsive transcription factors known as *RYPS1-4*[37-39]. These transcription factors work together to upregulate the production of yeast-specific transcripts that aid *Hc* during host infections.

Yeast-specific transcripts include α-glucan synthase, which is required for synthesis of α-glucan. Some *Hc* yeast strains are coated with α-glucan, which shields an inner layer of β-glucans. The α-glucan prevents the detection of β-glucan by the macrophage pathogen recognition receptor Dectin-1[40]. *Hc* yeast also secrete a glucanase, Eng1, that trims the β-glucans to prevent detection by the host[41]. This strategy permits *Hc* to be phagocytosed by immune cells and go undetected.

Inside of host cells, *Hc* must counteract immune defense strategies to survive and replicate. One defense strategy used by host cells is the release of reactive oxygen species (ROS). *Hc* yeast produce the extracellular superoxide dismutase, Sod3, as well as two catalases, an extracellular CatB and an intracellular CatP, to combat ROS in the cell [42, 43]. Within the phagosome, *Hc* yeast must acquire necessary nutrients for survival. Sequestration of nutrients is a common strategy used by host immune cells to combat infections. Within the phagosome, a nutritionally limited compartment, the yeast must acquire iron, zinc, and copper. *Hc* secretes siderophores like Sid1 to take up ferric iron directly[44] and a zinc transporter, Zrt2, to acquire zinc from its environment[45].

The most well studied virulence factor is calcium binding protein 1 (Cbp1). This 78 amino-acid virulence factor was first identified in 1997. It is the most abundant protein made by *Hc* yeast, and it is not expressed by hyphal cells[46]. Recent work identifies Cbp1 as a homodimer with a novel structural fold (the binocular fold) and no known domains[47]. Cbp1 is dispensable for intracellular fungal burden, but absolutely required for

macrophage lysis, indicating that this lysis defect is independent of intracellular growth[48]. The lack of lysis seems to be due to the inability of the yeast to induce the integrated stress response (ISR)[49]. The ISR is an intracellular cytosolic cascade induced during cellular stresses such as amino acid starvation, ER stress, and iron deprivation[50]. When the stress is not resolved, ISR activation leads to apoptosis, partially through caspase-3/7 activation and the oligomerization of Bax/Bak. The induction of this cascade during *Hc* infection is dependent on Cbp1. Mutation of host factors involved in the ISR like the transcription factor C/EBP homologous protein (*CHOP)* or the pseudokinase Tribbles homologue 3 (*TRIB3*) make macrophages partially resistant to *Hc* infection. Mice deficient in *CHOP* are less susceptible to *Hc* infection, indicating that this host pathway is relevant both in macrophages and in vivo during the mouse model of infection. Importantly, the mechanism by which Cbp1 induces this cytosolic cascade is still unknown. Recently published work showed Cbp1 accesses the host cytosol through an unknown mechanism[47]. It is unclear whether there is a generalized way *Hc* delivers effectors into the host cytosol or whether there is a specialized mechanism by which Cbp1 accesses the cytosol. Additionally, one of the major questions regarding *Hc* pathogenesis is whether effectors other than Cbp1 exist, and how to identify them.

Knottins

Using criteria identified in the plant fungal pathogen literature, we have been able to identify many putative effectors. We identified a number of proteins that were predicted to be secreted, were small in size (less than 250 amino acids), and exhibited a conserved C-terminal 6-cysteine spacing pattern reminiscent of some plant fungal pathogen effectors[30]. Examining existing Hidden Markov Models (HMM) of cysteine-rich protein

domains, we determined the 6-cysteine motif had homology to an existing knottins gene family called Fungi1[51]. Knottin domains are comprised of three interwoven disulfide bonds that form one of the smallest known stable globular domains. This feature makes these proteins extremely resistant to chemical, heat, and proteolytic stresses[52]. Proteins in the knottin family can be found in animals, insects, plants, and fungi[53]. Functional studies have shown knottins can act as ion channel inhibitors[54], insecticides[55] and protease inhibitors[56]. Knottins are intriguing candidates for novel virulence factors in *Hc*.

The founding member of the fungal knottin family, Fungi1, is the effector Avr9 from the tomato blight fungal pathogen *Cladosporium fulvum*[16, 17]. When *C. fulvum* infects tomato plants it can cause widespread disease. However, some strains of *C. fulvum* carry "avirulent genes" (*AVR* genes) that encode proteins that trigger recognition by the tomato plant if the plant carries the corresponding resistance genes. This recognition triggers a rapid host cell death at the site of infection, preventing further spread of the pathogen. If the plant lacks the resistance gene, these AVR effectors can promote pathogenesis of the fungus. In the case of Avr9, its mechanism of action is still unknown. Interestingly, our lab observed a number of years ago that there are at least 12 predicted proteins in the *Hc* G217B genome with homology to the Fungi1 family of proteins.

In the first part of this work, we use bioinformatics to mine the *Hc* genome to generate candidate lists of putative effectors. From this candidate list, and in combination with our previous observations, we identify a handful of the effectors with homology to knottins. In total, the *Hc* genome encodes at least 26 putative knottins, which indicates huge expansion of this protein family. Furthermore, we observe that this massive expansion is unique to *Histoplasma* and is not observed in other fungi, even closely

related species. This unique expansion suggests that knottins play a key role in *Hc* biology. Here we use genetic and cell biological approaches to further explore the role and function of four putative knottins in *Hc* infections. We observe that the knottins are required for *Hc* virulence in both macrophages and in mice.

Chapter 2: Identification of putative effectors reveals homology to the knottin gene family

Introduction:

A handful of effectors have been identified to be important for *Hc* pathogenesis. To identify novel *Hc* effectors, we used guidelines from the field of plant fungal pathogens, where many effectors have been identified. Based on plant fungal effectors, we focused on four criteria to generate a list of putative *Hc* effectors: small, secreted, yeast-expressed, and enhanced cysteine content (Table 2.1).

The morphological transition from the environmental form to the yeast form of *Hc* is regulated by a network of transcription factors known as *RYPS1-4*[37-39]. These TFs are required for yeast-phase growth and the expression of known virulence factors. To give an overview of our pipeline, we determined which yeast-specific transcripts encoded predicted proteins that were less than 250 amino acids in size and predicted to be secreted. We also considered high cysteine content, which is thought to provide proteins with stability through the formation of disulfide bridges. Using these guidelines, we generated a list of putative effectors.

Guidelines for identifying putative effectors

The two morphological states of *Hc*, yeast and hyphae, have differential expression profiles[30]. The *Hc* yeast transcription program is regulated by a network of temperature responsive transcription factors known as *RYPS1-4*[37-39]. These transcription factors work together to upregulate the production of yeast specific transcripts that aid *Hc* during host infections. In total we predict *Hc* has approximately 9014 protein-coding transcripts of which approximately ~1401 are direct targets of at least one Ryp TF (Ryp1, 2, 3 and/or 4). Of the 9014 transcripts, 3798 are predicted to encode a protein that is

smaller than 250 amino acids and ~139 show yeast-specific expression. Similarly, ~927 transcripts are predicted to encode secreted proteins based on the Phobius algorithm[57, 58]. Taken together, there are ~100 transcripts that are predicted to encode small, secreted proteins with yeast-specific expression (Figure 2.1).

Lastly, to further refine our list of putative effectors, we included the criterion that they contain at least 4 cysteines. Most of the *Hc* predicted proteins (~60%) have very few cysteines (between 0-2 cysteines) whereas ~40% of the predicted proteins (4005 proteins) contain 4 or more cysteines. Taking all criteria together, we are left with 51 effector candidates (Figure 2.2).

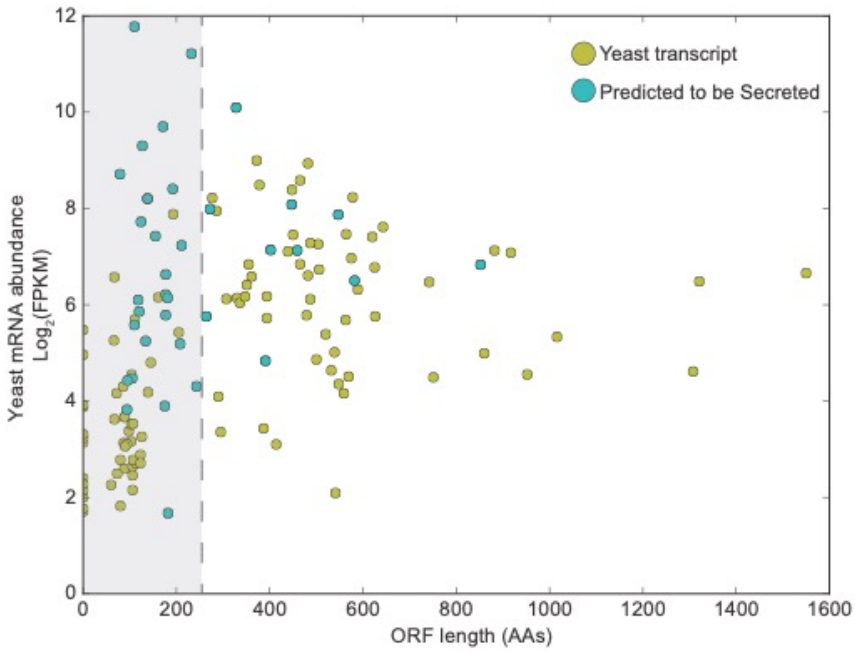

Figure 2.1: Expression profile comparisons reveal many putative small, secreted effectors. Plot showing mRNA abundance (Log_2 (FPKM) normalized) as a measure of ORF length (in amino acids). Each yellow dot represents yeast transcripts. Teal dots denote yeast transcripts that are predicted to be secreted. Grey box denotes yeast specific transcripts that are <250 amino acids in length.

Table 2.1: Criteria for identifying *Hc* effectors. Putative effectors were selected if they were small (< 250 amino acid), secreted (signal sequence prediction by Phobius), yeast specific expression (contain upstream RYP binding event) and cysteine-rich (≥ 4 cysteines).

Criteria	Description of criteria
1. Small protein	<250 amino acids
2. Secreted	Phobius signal sequence prediction
3. Ryp Associated	Has upstream RYP binding event, yeast expressed
4. Cysteine-rich	≥ 4 cysteines

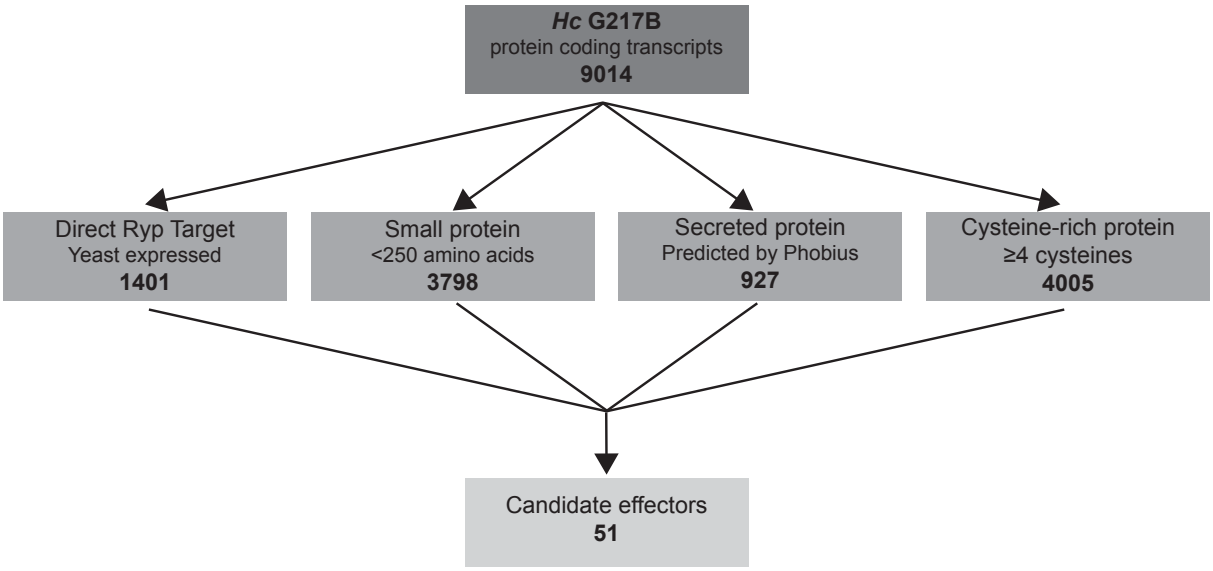

Figure 2.2: Comparison of proteins identified based on effector criteria.
Hc contains approximately 9014 protein coding transcripts. Filtering on each of the four criteria gives different sets of genes. *Hc* genome encodes ~4005 protein coding transcripts that have at least 4 cysteines, ~3798 protein coding transcripts that are smaller than 250 amino acids, ~927 protein coding transcripts that are predicted to be secreted and ~1401 protein coding transcripts that are direct targets of the Ryp1, 2, 3 and/or 4. Applying all 4 criteria gives 51 putative effectors.

List of putative effectors

The criteria listed in Table 2.1 and Figure 2.2 generates a list of 51 putative effectors (Figure 2.3). Notably, this list includes effectors that have been previously identified, such as Cbp1 and Sod3, corroborating the validity of the algorithm. To further narrow down this list for more detailed exploration we looked for commonalities amongst the 51 putative effectors. We observed that several of the effectors on this list had previously been identified as having homology to a preexisting gene family called the knottins. Knottins are characterized by the presence of a conserved C-terminal 6-cysteine spacing pattern reminiscent of some plant fungal pathogen effectors[30]. Knottin domains are comprised of three interwoven disulfide bridges. This feature makes these proteins extremely resistant to chemical, heat, and proteolytic stresses[52]. During annotation of the *Hc* transcriptome in a previous study, the Sil lab had identified 12 putative knottins in the *Hc* G217B genome that resembled the Fungi1 family of knottins[30] (Figure 2.4A).

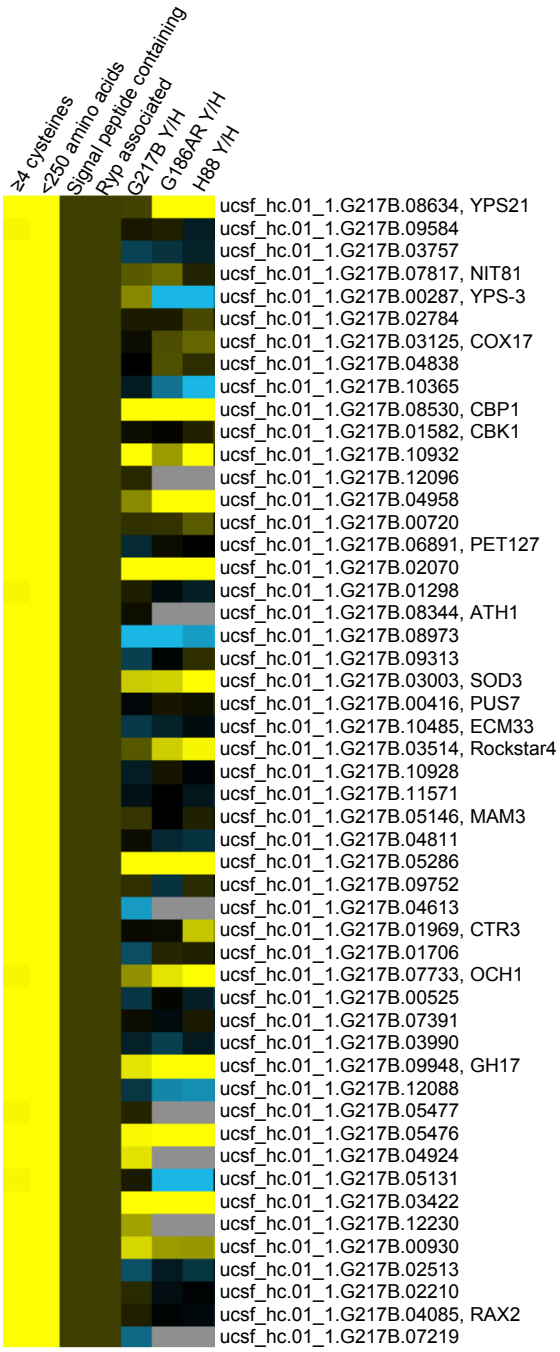

Figure 2.3: List of putative *Hc* effectors. 51 putative effectors were identified. The first four columns denote that each putative effector fulfilled the criteria set in Table 2.1. Each effector has at least 4 cysteines, is smaller than 250 amino acids, contains a signal peptide and is RYP associated respectively. The next three columns denote whether that effector's transcript expression is up (yellow) or down (blue) in yeast relative to hyphae in the different *Histoplasma* species; G217B, G186AR or H88. Listed are the predicted transcript names for G217B along with any available annotated names.

KNOTTIN Finder identified 26 putative knottins

We hypothesized that other knottins might be present in the *Hc* genome. We wrote an unbiased and naïve algorithm called KNOTTIN Finder to discover other putative knottins. The algorithm translates all contigs from the G217B *Hc* genome and translates them into all possible reading frames. Each contig is segmented along stop codons. Next, it looks for all cysteines within each predicted protein and selects those with at least 6-cysteines. Importantly, the algorithm compares all contigs with the Fungi1 knottin family. Lastly, it filters predicted proteins that are less than 250 amino acids, thereby selecting for small proteins (Figure 2.4B). Interestingly, using this code we were able to identify 26 putative knottins. This algorithm can detect putative knottins even in unannotated regions of the genome. Importantly, if we query genome-wide ribosomal profiling data, we find ribosomal occupancy signal in yeast-phase cells, suggesting that the predicted knottins from KNOTTIN Finder represent true protein-coding transcripts (Figure 2.4C). Listed in Table 2.2 are all 26 knottins with their predicted gene and transcript names in G217B *Hc*. The table also lists whether the knottin had been previously identified during annotation of the genome in our lab or whether it was identified by the KNOTTIN Finder algorithm. Lastly, phylogenetic analysis determined that the 26 knottins fall into 15 distinct gene clades, which are denoted in the last column of Table 2.2. We wondered what the genome organization of the 26 putative knottins were. Finally, by examining the genome location of each knottin on the *Hc* chromosomal map, we observed that the knottins are evenly distributed across the genome (Figure 2.5).

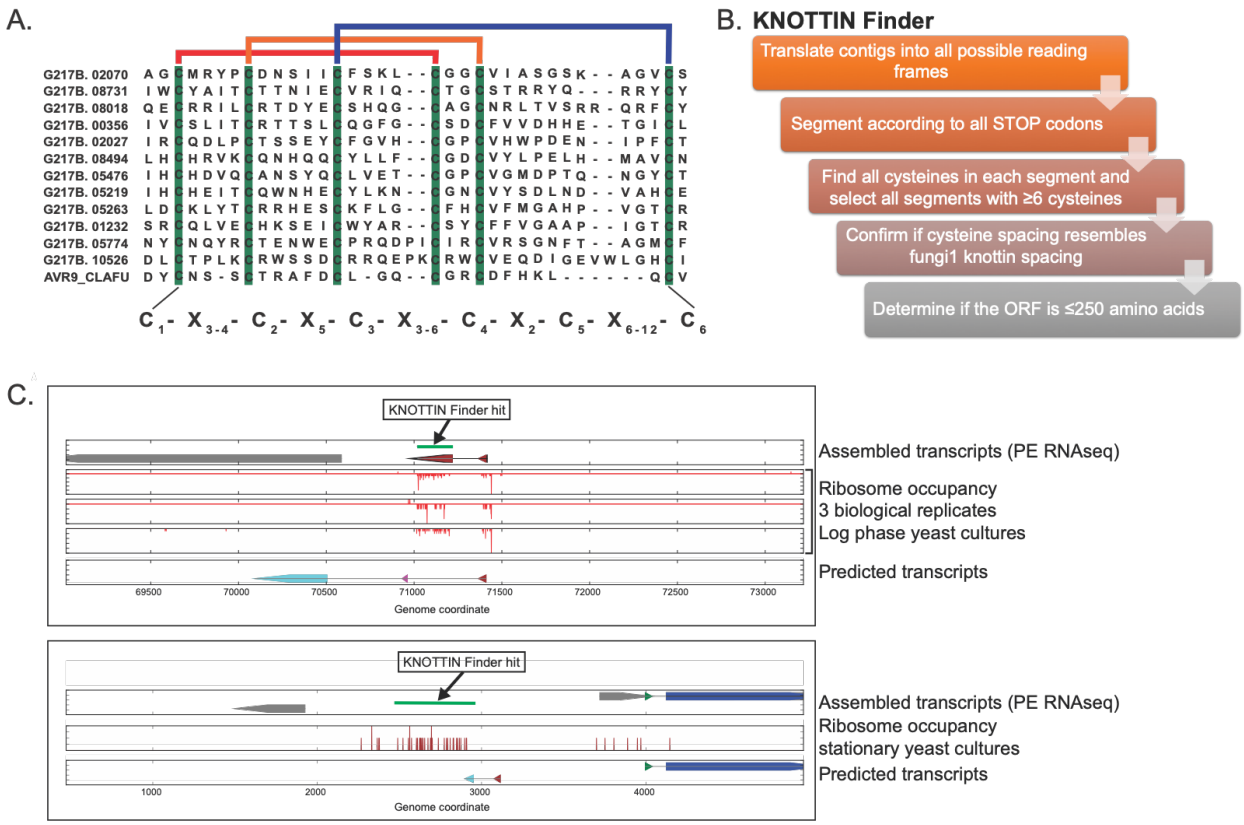

Figure 2.4: 26 putative knottins were identified in the *Hc* genome. (A) Figure modified from Gilmore, S. et. al. 2015 where 12 knottins were originally identified. Protein alignment of C-terminal region of putative *Hc* knottins. Green denotes the 6-cysteine spacing pattern. Avr9 from *C. fulvum* is aligned as a reference. The knottin spacing pattern is referenced below. Above cysteines that make disulfide bonds are connected (red, orange, and blue line). (B) Simplified diagram of steps in KNOTTIN Finder algorithm. (C) Examples of putative knottins identified by KNOTTIN Finder. Top panel is representative of knottin from a previously annotated gene. Bottom panel is representative of a knottin from an unannotated region. Green bar denotes KNOTTIN Finder hit. Show is the assembled transcripts from paired-end RNAseq data, ribosomal occupancy from 3 biological replicates and the predicted transcripts.

Table 2.2: List of putative knottins with gene names.

Knottins	Gene Prediction Name	Transcript Name	SG Paper or Knottin Finder	Name	Clade
knottin_HcG217B_000	HISTO_GY.Contig471.eannot.1357.final_new	ucsf_hc.01_1.G217B.05774	SG PAPER		4
knottin_HcG217B_001		ucsf_hc.01_1.G217B.08494	SG PAPER		11
knottin_HcG217B_002	HISTO_ZU.Contig65.Fgenesh_Neurospora.61.final_new		KNOTTIN FINDER		5
knottin_HcG217B_003	HISTO_ZU.Contig65-snap.210.final_new		KNOTTIN FINDER		5
knottin_HcG217B_004	HISTO_ZU.Contig65.Fgenesh_histo.38.final_new	ucsf_hc.01_1.G217B.11056	KNOTTIN FINDER		4
knottin_HcG217B_005	HISTO_FX.Contig167.Fgenesh_histo.13.final_new	ucsf_hc.01_1.G217B.04359	KNOTTIN FINDER		7
knottin_HcG217B_006	HISTO_BP.Contig459.eannot.1514.final_new	ucsf_hc.01_1.G217B.01232	SG PAPER	KNOT2	9
knottin_HcG217B_007	HISTO_ZL.Contig1117-snap.1.final_new		KNOTTIN FINDER		8
knottin_HcG217B_008	HISTO_FE.Contig19.Fgenesh_histo.274.final_new		KNOTTIN FINDER		11
knottin_HcG217B_009	HISTO_DF.Contig537.eannot.1411.final_new	ucsf_hc.01_1.G217B.02070	SG PAPER	KNOT1	12
knottin_HcG217B_010		ucsf_hc.01_1.G217B.02027	SG PAPER		11
knottin_HcG217B_011			KNOTTIN FINDER		7
knottin_HcG217B_012	HISTO_AS.Contig189.eannot.1025.final_new	ucsf_hc.01_1.G217B.00356	SG PAPER		9
knottin_HcG217B_013	HISTO_ZL.Contig1131-snap.93.final_new	ucsf_hc.01_1.G217B.08731	SG PAPER		14
knottin_HcG217B_014		ucsf_hc.01_1.G217B.04757	KNOTTIN FINDER		10
knottin_HcG217B_015		ucsf_hc.01_1.G217B.08018	SG PAPER		14
knottin_HcG217B_016		ucsf_hc.01_1.G217B.04212	KNOTTIN FINDER		11
knottin_HcG217B_017	HISTO_ZT.Contig174.eannot.1455.final_new	ucsf_hc.01_1.G217B.10526	SG PAPER		5
knottin_HcG217B_018	HISTO_KK.Contig134.Fgenesh_histo.2.final_new		KNOTTIN FINDER		11
knottin_HcG217B_019	HISTO_LS.Contig117-snap.1.final_new	ucsf_hc.01_1.G217B.08080	KNOTTIN FINDER		5
knottin_HcG217B_020	HISTO_GX.Contig297.Fgenesh_histo.73.final_new	ucsf_hc.01_1.G217B.05263	SG PAPER		14
knottin_HcG217B_021		ucsf_hc.01_1.G217B.05219	SG PAPER		11
knottin_HcG217B_022	HISTO_GL.Contig296.eannot.1373.final_new	ucsf_hc.01_1.G217B.04958	KNOTTIN FINDER		10
knottin_HcG217B_023	HISTO_GY.Contig460.eannot.1679.final_new	ucsf_hc.01_1.G217B.05476	SG PAPER	KNOT3	11
knottin_HcG217B_024	HISTO_BM.Contig14-snap.1.final_new	ucsf_hc.01_1.G217B.00750	KNOTTIN FINDER		5
knottin_HcG217B_025	HISTO_KF.Contig470.eannot.1024.final_new	ucsf_hc.01_1.G217B.06783	KNOTTIN FINDER	KNOT4	6

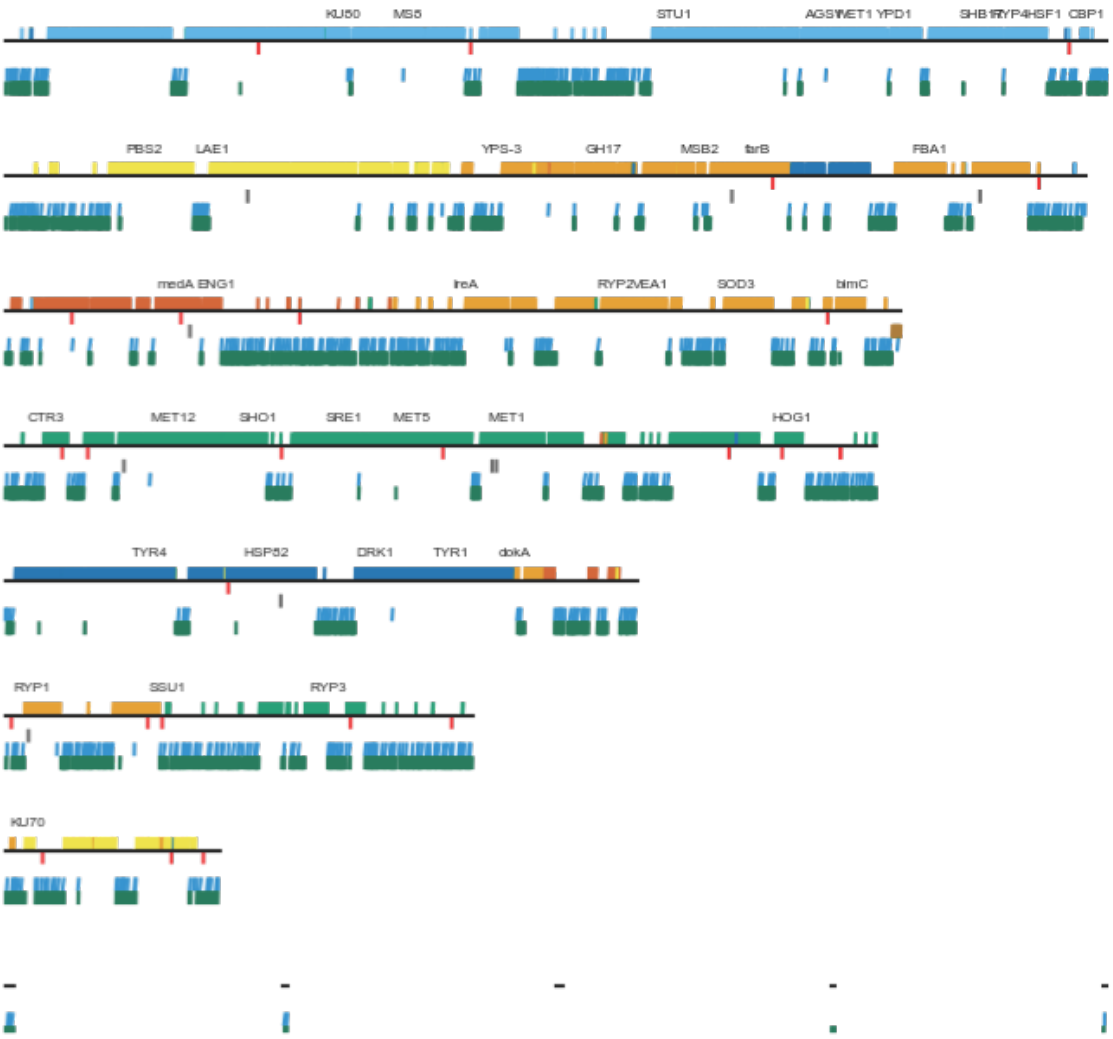

Figure 2.5: Random distribution of knottins throughout *Hc* genome. Diagram of the seven *Hc* G217B chromosomes assembled from Nanopore sequencing reads. Marked in red below each chromosome are the knottins. They are randomly distributed across the genome. Blue and green refers to transposons and black tick marks indicate rRNAs. Genes of interest are labeled.

Expansion of knottins in Histoplasma species

We next wondered whether the presence of 26 knottins was common across fungi. We ran our knottin finder algorithm against ≥600 fungal genomes to look for putative knottins within different genomes. Most of these genomes were present in the ENSEMBL database. A few were present only in GenBank, including the *Cladosporium fulvum* genome that encodes AVR9, the founding member of the Fungi1 family of knottins.

We performed a phylogenetic analysis of all fungal genomes vs. the knottins we identified in *Hc,* which are organized into 15 distinct clades (Figure 2.6). The intensity of the red indicates how many knottins of that clade were found in a particular genome. Surprisingly, we observed that the knottin family is greatly expanded in *Histoplasma* species relative to other fungi. *Hc* species typically have 22-27 knottins per genome. Closely related thermally dimorphic fungi also contain knottins. For example, *Blastomyces* species have 2-3 knottins per genome, *Paracoccidioides* species have 4-6, and *Emergomyces* species have 10-17 knottins. Outside of the thermal dimorphs, few knottin genes were identified (Figure 2.6). The large expansion of knottins in the *Hc* genome suggests that they play a key role in *Histoplasma* biology. This result reinforces our interest in these knottin proteins as putative *Hc* effectors.

Figure 2.6: Phylogenetic analysis reveals massive expansion of knottins within *Histoplasma* species. Phylogenetic analysis of knottins in 66 representative fungal genomes. *Hc* G217B knottins fall into 15 distinct gene clades. The intensity of the red indicates the number of knottins present in each clade per genome. Teal square denotes Avr9 from *C. fulvum*. Branch lengths are not to scale.

Discussion and future directions:

This work highlights our efforts to more comprehensively mine the *Hc* genome for novel effectors. For many years the *Histoplasma* field has focused on a handful of secreted effectors. Effectors such as Cbp1 and Yps-3 have been shown to play a role in virulence, but we are not any closer to determining their function. We decided to look to the field of plant fungal pathogens to develop criteria for putative effectors. We used four criteria to define putative effectors: small, secreted, direct Ryp targets, and enhanced cysteine content. One caveat to this method of identifying effectors is that if the effector does not have a canonical signal sequence or is secreted by another method like through extracellular vesicles (EVs) it will not be part of our list but could still be an important effector. Regardless of potential caveats, this method generated a list of 51 putative effectors.

We note that using bioinformatic tools to generate lists of putative effectors is a relatively straightforward way to generate candidates for further study. Generally, genome organization/location can suggest the presence of effector regulons. Additionally, analysis of protein sequence similarities can give insight into potential conservation and evolutionary gain and/or loss. Algorithms such as AlphaFold can be used to predict protein structure and functions. This work sets up a straightforward framework from which to explore novel effectors and has generated a list of interesting proteins to explore further in future work.

Chapter 3: Characterization of *KNOT1-4* reveals their roles in *Hc* pathogenesis of macrophages

Introduction

With the identification of the knottin gene family we wanted to explore their function and potential role in *Hc* pathogenesis. We needed to prioritize which of the 26 putative knottins identified in Chapter 2 to characterize. Four knottins representing four different *Hc* clades were chosen and named *KNOT1-4*. Protein alignments of the C-terminal knottin spacing compared to *C. fulvum* Avr9 is shown in Figure 3.1A. Ribosomal profiling indicates ribosomal occupancy during yeast phase growth (red signal) for all four knottin transcripts (Figure 3.1B), highlighting their preferential expression in yeast over hyphae (shown in green). Additionally, paired-end sequencing data from yeast and hyphal transcriptomes shows the extent of differential expression of Knot1-4 transcripts (Figure 3.1C)[30]. The clade designation for Knot1-4 is shown in Figure 3.2. A comparison of the C-terminal region from Knot1-4 in the *Hc* strain G217B to sequences in multiple *Hc* isolates identified corresponding orthologs or paralogs in these other *Histoplasma* species. Knot1 and Knot4 are highly conserved at the protein level across the different species, only one copy of Knot1 and Knot4 is present per genome. Knot2 and Knot3 are less conserved across the different *Histoplasma* species. Within the G217B genome Knot2 has one paralog and Knot3 has 6 paralogs. This is important, as paralogs may be functionally redundant with each other. Lastly, Knot1 was of interest because it was previously identified in an insertional mutagenesis screen to identify mutants that fail to lyse macrophages[48].

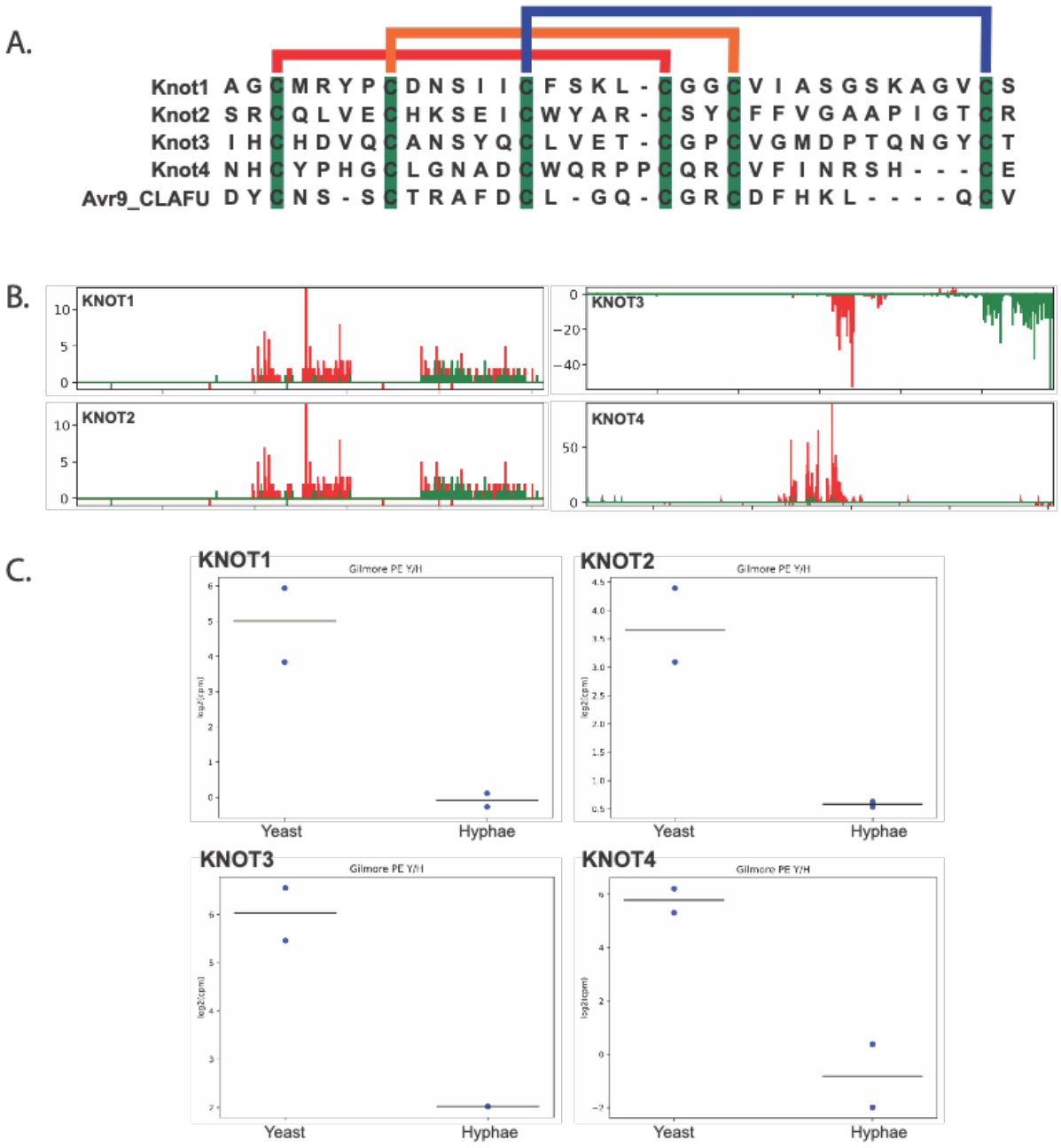

Figure 3.1: Protein alignment of knottin motif and ribosome profiling for Knot1-4. (A) Protein alignment of the C-terminal region for Knot1-4. Avr9 from *C. fulvum* used a reference for the Fungi1 knottin cysteine spacing pattern. Green denotes cysteines. Above cysteines that make disulfide bonds are connected (red, orange, and blue line). (B) Ribosome profiling plots for Knot1-4. Red signal denotes ribosome occupancy in the yeast form. Knot1-4 are yeast phase specific proteins. (C) Paired end sequencing results from yeast and hyphae showing Log_2(CPM) reads for Knot1-4. Knot1-4 are highly expressed in yeast and very lowly expressed in hyphae.

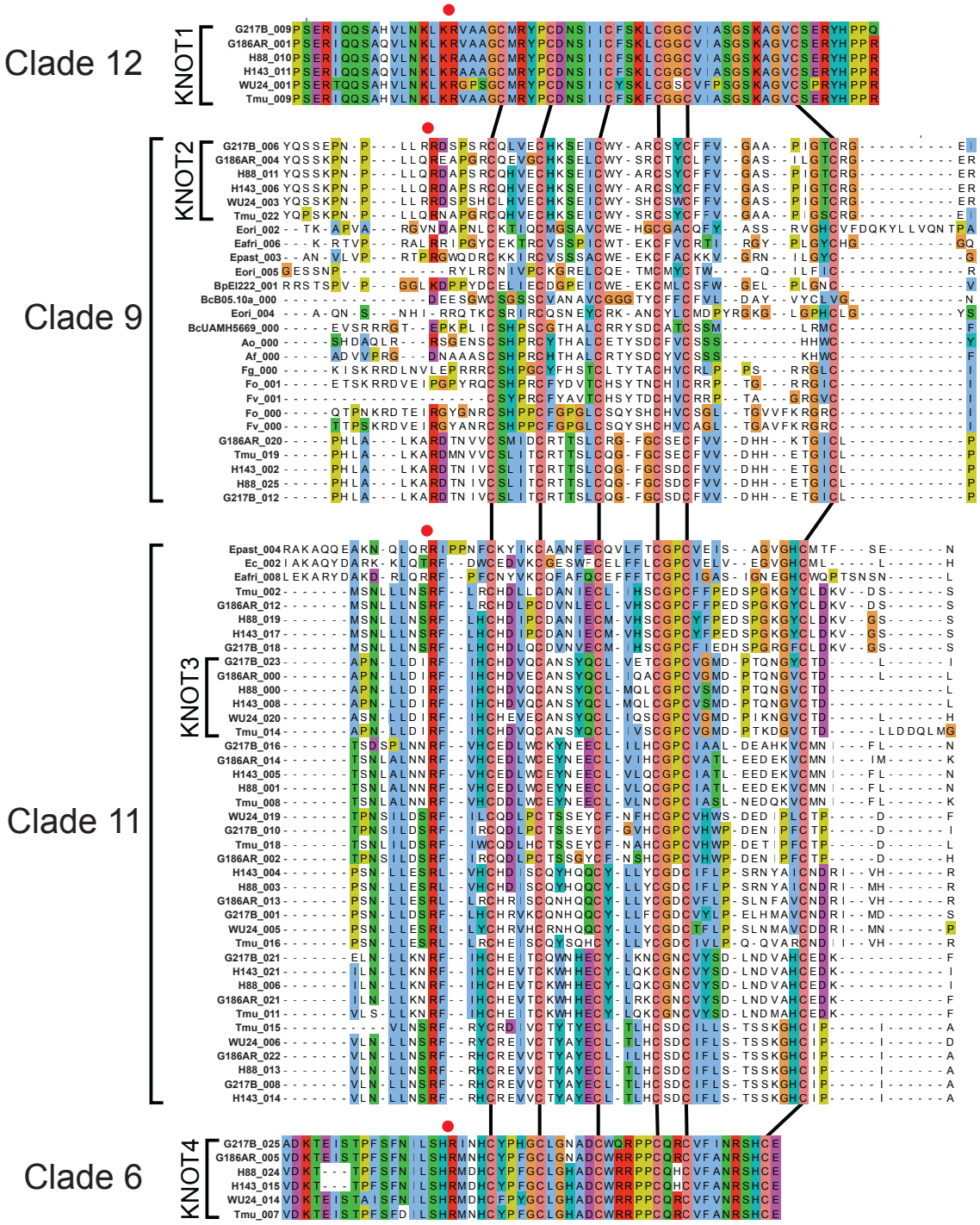

Figure 3.2: Protein alignment of Knot1-4 in different gene clades. Protein alignments of Knot1-4 across different *Hc* species. Knot1 and Knot4 have high conservation across the different *Hc* species and only one copy is found in each genome. Knot4 is the homolog of Avr9 from *C. fulvum*. Knot2 and Knot3 are less conserved at the protein sequence across the different species. The 6-cysteine spacing is denoted by the lines between clades. The red dot indicates a conserved Arginine, a positively charged residue.

Knot1-4 are secreted by Hc yeast and access the macrophage cytosol

We wanted to first confirm experimentally that Knot1-4 are secreted. We tagged each of these knottins with a C-terminal 3X-FLAG tag as it's relatively small and works well for Western blot detection. A six-glycine linker was also incorporated to allow some flexibility between the knottin domain and the tag and to reduce potential interference by the tag. After introduction into *Hc,* culture supernatants from individual transformants were screened for expression of the FLAG-tagged knottin protein by SDS-PAGE followed by Western blot. Knot1-4 were detected in culture supernatants (Figure 3.3). All four knottins ran at the predicted size, ranging from 8-10kDa.

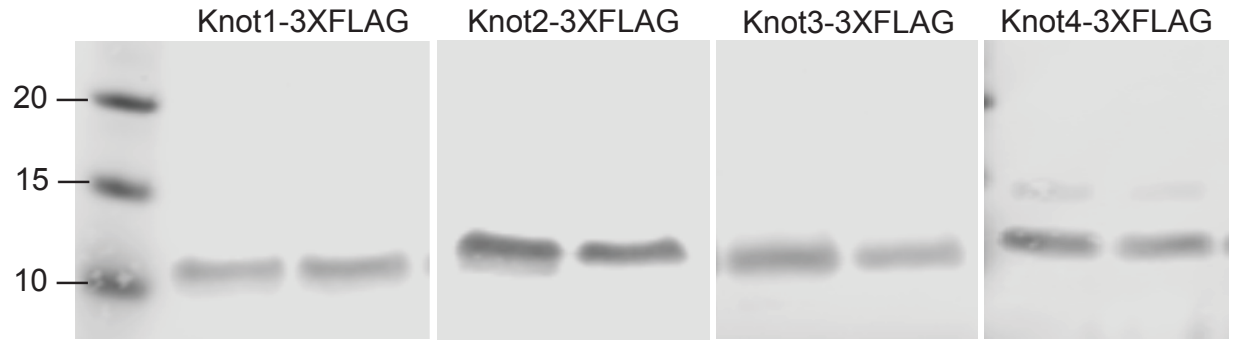

Figure 3.3: C-terminally 3X-FLAG tagged knottins are secreted into culture supernatants by *Hc* yeast. Two independent *Hc* colonies expressing Knot1-4 3X-FLAG are shown.

Next, to further explore the role of *KNOT1-4* as *Hc* effectors we wondered whether they accessed the macrophage cytosol during infection like Cbp1[47]. We used subcellular fractionation to probe for effectors in the macrophage cytosol after infection of murine bone marrow derived macrophages (BMDMs) with *Hc*. We infected at a multiplicity of infection (MOI) of 5 and collected infected cells at 24 hours post-infection. Cells were lysed by passaging them through a 27-gauge needle, which will lyse the cell plasma

membrane but leave the internal membranous organelles intact. Samples were then subjected to an ultra-high centrifugation at 100,000 x g for 2 hours at 4°C to separate the cytosolic fraction from the membrane fraction. Each fraction was subjected to SDS-PAGE and Western blotting with the FLAG antibody. To assess the purity of the fractionation, we followed α-tubulin to mark the cytosolic fraction and calnexin, an ER membrane protein, to mark the membrane fraction. Additionally, we probed for Cbp1, which was established as accessing the host cytosol in previous work. Each fractionation experiment included BMDMs that were infected with wild-type untagged *Hc*, the knottin 3X-FLAG-tagged strains, or mock-infected BMDMs. Remarkably, Knot1, 2, 3 and 4 were detected in the host cytosolic fraction from infected cells, much like Cbp1 (Figure 3.4). We did not observe any FLAG signal in the membrane fraction, suggesting that Knot1-4 are enriched in the host cytosol during infection.

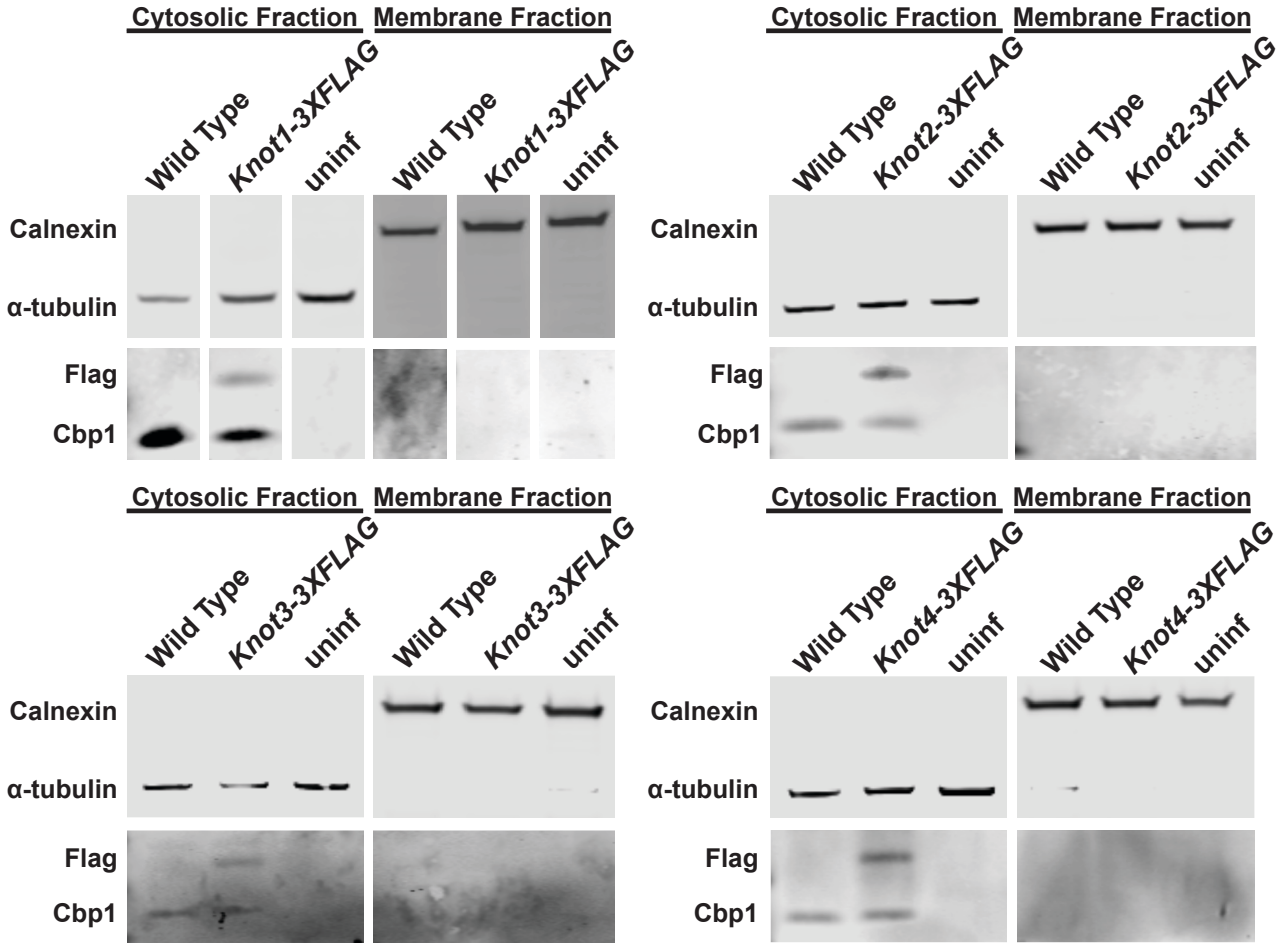

Figure 3.4: Knottins access the host cytosol. Western blot of fractionated lysates was run using α-tubulin antibody as a marker for the cytosol and calnexin antibody as a marker for the membrane fraction. Cbp1 custom antibody was used as a positive control for effectors that access the cytosol. Anti-FLAG antibody was used to detect tagged knottins. Wild type *Hc* (*ura5Δ* + URA5) was used in every fractionation. Knot1-3XFLAG *Hc* (*ura5Δ* + KNOT1-3XFLAG), Knot2-3XFLAG *Hc* (*ura5Δ* + KNOT2-3XFLAG), Knot3-3XFLAG *Hc* (*ura5Δ* + KNOT3-3XFLAG), and Knot4-3XFLAG *Hc* (*ura5Δ* + KNOT4-3XFLAG) were used in fractionation experiments. BMDMs were infected at MOI=5 and collected 24hpi.

Hc deletion mutants were generated using CRISPR-Cas9

To directly explore the role of Knot1-4 in virulence we generated deletion mutants using CRISPR-Cas9. This technology is relatively new in *Hc.* Using an episomal plasmid that expresses Cas9 and two guides that target the gene of interest, it is possible to generate targeted deletions in the *Hc* genome. We presume that non-homologous end

joining fuses the two chromosomal ends together after Cas9-directed excision, thereby eliminating the gene of interest. Table 3.1 lists the protospacer sequences used to target *KNOT1-4*. A diagram of *KNOT1-4* gene loci shows the approximate location of the cut sites being targeted by Cas9 (Figure 3.5A). Importantly, cut sites were chosen to be as close as possible to the start and end of the coding sequence of interest depending on the availability of the PAM sequence (NGG). Usually, the targeted cut site was within 200bp of the start and stop of the coding sequence. Episomal plasmids carrying Cas9 and the appropriate guides were transformed into *Hc* and colonies were screened using PCR to identify isolates that no longer carried the wild-type locus for the gene of interest.

Table 3.1: List of guide RNA protospacers used to generate deletion mutants.

Knottin gene	Protospacer sequence	PAM sequence
Knot1	ATCAACCGATATATAAGACT	TGG
Knot1	TGCGCTATATTGTAATTAGA	CGG
Knot2	TCTATCTGGCGAAACATTG	GGG
Knot2	TTCGTCGGCGCCGCTCCAAT	CGG
Knot3	ACAACTAATATTCCGATTGA	AGG
Knot3	ACGTGACCGTTTAGATCACG	TGG
Knot4	TCCAATATGATAAAAGTGGA	AGG
Knot4	TTGAATTCTATATCAATCGC	TGG

To validate final mutants, three different PCR reactions were set up using genomic DNA from wild type *Hc* or the CRISPR deletion mutants. Primers for these reactions are listed in Table 5.1. Primers were designed to bind externally to the targeted cut site, internally to the cut site, or spanning either side of the 5' or 3' cut site. Expected results are shown in Figure 3.5B. This diagram shows roughly the positions of each primer used to screen through deletion mutants. PCR amplification of the wild-type locus of *KNOT1* using external primers produced a ~1000 bp product. In the final deletion mutant, external primers produced a PCR product that is ~300 bp. PCR amplification of the wild-type locus

of *KNOT1* using one external primer and one internal primer produced a ~500 bp product. In the final deletion mutant, these primers yield no PCR product. PCR amplification of the wild-type locus of *KNOT1* using internal primers produced a ~400 bp product. In the final deletion mutant, internal primers produce no PCR product. The same was true for *KNOT2*, *KNOT3*, and *KNOT4* as shown in Figure 3.5B. Final mutants were also validated by whole genome sequencing (WGS), data not shown.

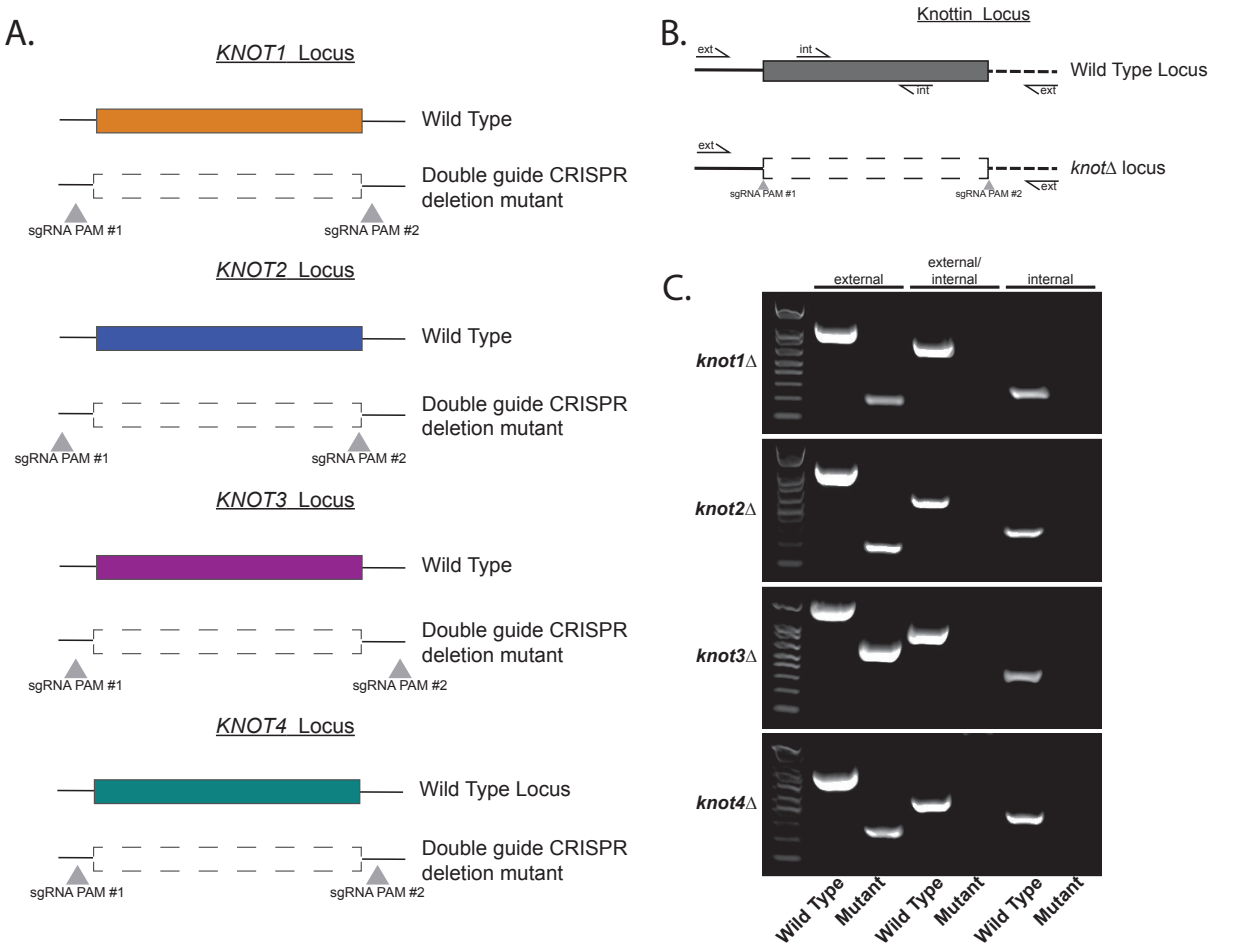

Figure 3.5: CRISPR-Cas9 was used to generate deletion mutants of *KNOT1-4* that were validated by PCR. (A) Cartoon depiction of *KNOT1-4* gene loci and approximate location of both sgRNAs that target Cas9 to induce a cut in the genome. (B) PCR schematic to validate final deletion mutants. (C) 1% agarose gel stained with ethidium bromide shows final mutants are clean deletions. Genomic DNA was extracted from wild type *Hc* (*ura5Δ* + URA5), *knot1Δ* (*ura5Δ, knot1Δ* + URA5), *knot2Δ* (*ura5Δ, knot2Δ* + URA5), *knot3Δ* (*ura5Δ, knot3Δ* + URA5), and *knot4Δ* (*ura5Δ, knot4Δ* + URA5) mutant *Hc*.

Finally, complementation strains were generated for each deletion mutant to validate that phenotypes were due to deletion of the gene of interest and not CRISPR off-target effects. Each coding sequence, including native 5' and 3' UTRs, was cloned into an episomal plasmid (pDG33). Plasmids were linearized and transformed into *Hc*. *KNOT1* complementation construct included ~2.5kb of its native 5' UTR and ~2.2kb of its 3' UTR. *KNOT2* complementation construct included ~4kb of its native 5' UTR and ~0.7kb of its 3' UTR. *KNOT3* complementation construct included ~1kb of its native 5' UTR and ~1kb of its 3' UTR. *KNOT4* complementation construct included ~2kb of its native 5' UTR and ~1.5kb of its 3' UTR. Importantly, the 5' UTR for all complementation constructs included any upstream binding sites for the Ryp transcription factors that drive yeast-phase growth. Colonies were screened phenotypically and by qRT-PCR. Expression of the relevant knottin transcript was not observed in the corresponding mutant strain and was restored in the corresponding complementation strain at levels comparable to wild-type *Hc* (Figure 3.6). Primers used for this analysis are listed in Table 5.2. In data not shown, complementation plasmids were lost by growing the *Hc* strains in the absence of selection for the plasmid. In subsequent phenotypic studies, we confirmed that these strains regain the mutant phenotype, thereby validating that the wild-type phenotype is dependent on the complementation plasmid.

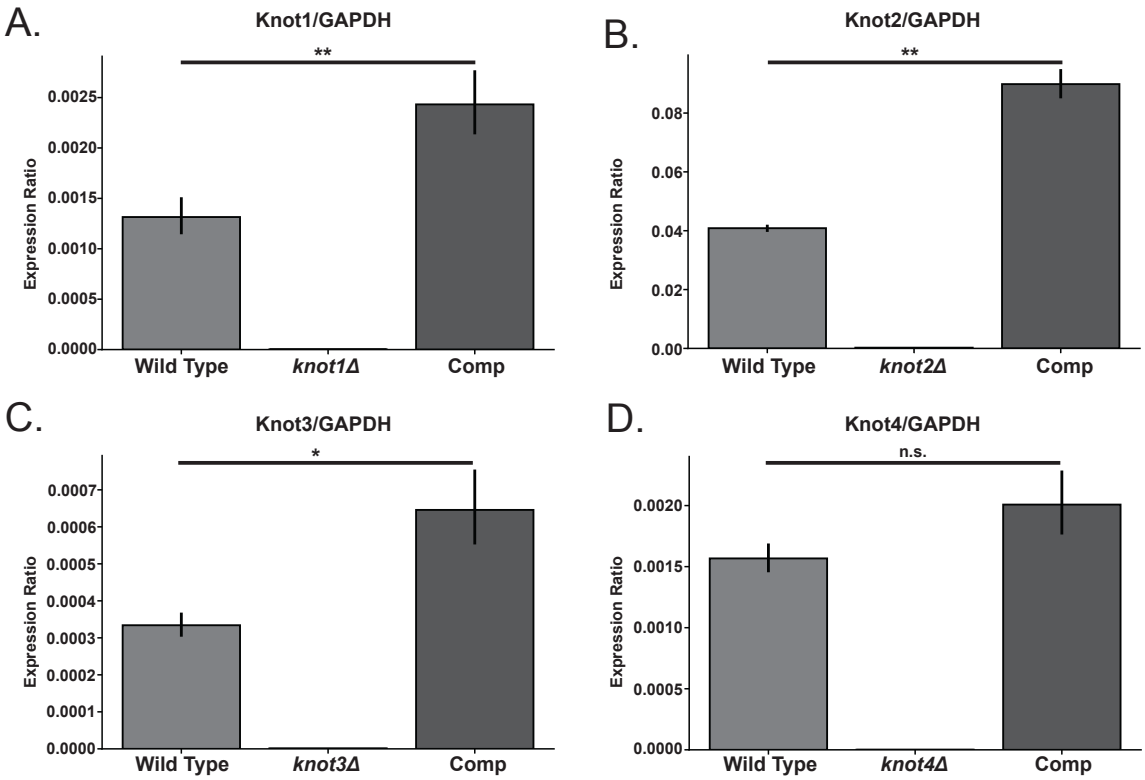

Figure 3.6: *knot1-4* deletion mutants were complemented and validated by qRT-PCR. (A) Expression of *KNOT1* relative to the housekeeping gene GAPDH. cDNA was made from wild type *Hc* (*ura5Δ* + URA5), *knot1Δ* (*ura5Δ, knot1Δ* + URA5), *and knot1Δ* complement *Hc* (*ura5Δ, knot1Δ* + KNOT1). (B) Expression of *KNOT2* relative to the housekeeping gene GAPDH. cDNA was made from wild type *Hc* (*ura5Δ* + URA5), *knot2Δ* (*ura5Δ, knot2Δ* + URA5), *and knot2Δ* complement *Hc* (*ura5Δ, knot2Δ* + KNOT2). (C) Expression of *KNOT3* relative to the housekeeping gene GAPDH. cDNA was made from wild type *Hc* (*ura5Δ* + URA5), *knot3Δ* (*ura5Δ, knot3Δ* + URA5), *and knot3Δ* complement *Hc* (*ura5Δ, knot3Δ* + KNOT3). (D) Expression of *KNOT4* relative to the housekeeping gene GAPDH. cDNA was made from wild type *Hc* (*ura5Δ* + URA5), *knot4Δ* (*ura5Δ, knot4Δ* + URA5), *and knot4Δ* complement *Hc* (*ura5Δ, knot4Δ* + KNOT4).

KNOT1 is required for macrophage lysis and intracellular growth

Next, we tested whether *KNOT1* is required for the yeast to grow *in vitro*. Wild type *Hc*, *knot1Δ* mutant *Hc* and *knot1Δ* complemented strain were grown in liquid HMM. At day 0, each strain was diluted to OD 0.05 in triplicate. All cultures were grown at 37°C and 5% CO_2 in an orbital shaker. Every 24 hours, 1 mL of culture was removed and vortexed for 30 seconds to disperse clumps and get an accurate optical density reading.

We observed that loss of *KNOT1* did not impact the yeast's ability to grow *in vitro* in HMM media. There was a subtle decrease in optical density observed in stationary phase, but it was not statistically significant (Figure 3.7A).

Next, we explored the role of Knot1 during infection of BMDMs. BMDMs were plated at $7.5x10^5$ cells per well in a 48-well dish. Approximately 24 hours later, BMDMs were either mock-infected or infected at a MOI of 0.5 with either wild type *Hc*, *knot1Δ* mutant *Hc* or the complemented strain. Lactate dehydrogenase (LDH) release assay was performed to quantify release of the cytosolic enzyme LDH from infected macrophages in supernatants collected over the course of the infection. We observed that *Hc* lacking Knot1 failed to lyse macrophages to same extent as either wild-type *Hc* or the complemented strain. However, unlike with the *cbp1Δ* mutant which triggers no host-cell lysis, the *knot1Δ* mutant has only a partial lysis defect (Figure 3.7B).

We then explored whether the inability to appropriately lyse macrophages was correlated with an inability to grow intracellularly. We infected BMDMs and quantified intracellular fungal burden. Samples were collected every 24 hours or until onset of macrophage lysis. Infected cells were lysed with ddH_2O to release intracellular *Hc. Hc* were plated on HMM agarose plates and incubated at 37°C, 5% CO_2 for 7-10 days to enumerate colonies. After lysis ensues, samples were no longer assessed since we cannot distinguish between extracellular and intracellular fungi in this assay. Therefore, in this particular infection, wild-type and complemented *Hc* were only examined until 72 hpi whereas the mutant was assessed until 96 hpi because no visible lysis had been observed. CFU analysis showed that *Hc* lacking Knot1 has an intracellular growth defect (Figure 3.7C).

Taken together these data indicate that *KNOT1* is dispensable for *in vitro* growth but required for both macrophage lysis and intracellular growth.

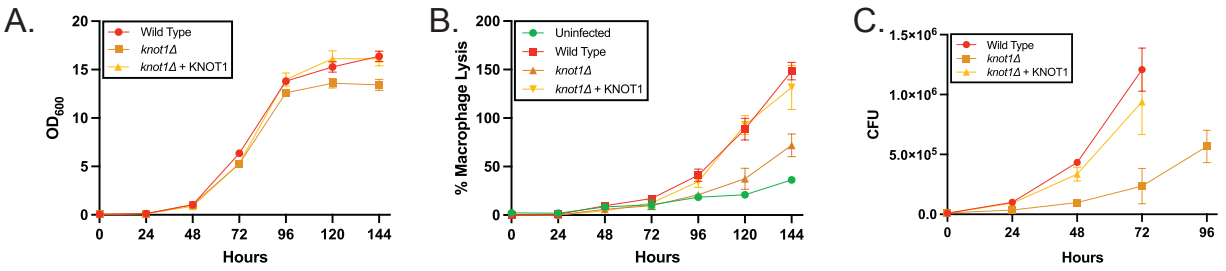

Figure 3.7: *KNOT1* is required for macrophage lysis and intracellular growth. (A) *In vitro* growth curve for wild type *Hc* (*ura5Δ* + URA5), *knot1Δ* mutant *Hc* (*ura5Δ*, *knot1Δ* + URA5), *knot1Δ* complemented *Hc* (*ura5Δ*, *knot1Δ* + KNOT1). *Hc* grown in HMM at 37°C, 5% CO_2 for 144 hours. Each strain grown in 100 mL in triplicate. (B) LDH release assay measuring % BMDM lysis over 144 hours. Uninfected BMDMs, or BMDMs infected with wild type *Hc* (*ura5Δ* + URA5), *knot1Δ* mutant *Hc* (*ura5Δ*, *knot1Δ* + URA5), *knot1Δ* complemented *Hc* (*ura5Δ*, *knot1Δ* + KNOT1) at MOI=0.5. All time points relative to time point 0 of uninfected cells lysed with 1% Triton in DMEM (total LDH). (C) Intracellular fungal burden for wild type *Hc* (*ura5Δ* + URA5), *knot1Δ* mutant *Hc* (*ura5Δ*, *knot1Δ* + URA5), *knot1Δ* complemented *Hc* (*ura5Δ*, *knot1Δ* + KNOT1). Time points counted until onset of macrophage lysis.

KNOT2 is required for macrophage lysis

We tested whether *KNOT2* was required for the yeast to grow *in vitro*. Wild type *Hc*, *knot2Δ* mutant *Hc* and *knot2Δ* complemented strain were grown in liquid HMM. At day 0, each strain was set to OD 0.05 and tested in triplicate. All cultures were grown at 37°C and 5% CO_2 in an orbital shaker. We observed that loss of *KNOT2* did not impact *Hc* ability to grow *in vitro* in HMM media (Figure 3.8A).

Next, we explored the role of *KNOT2* during infection of BMDMs. BMDMs were either mock-infected, or infected at a MOI of 0.5 with either wild type *Hc*, *knot2Δ* mutant *Hc* or the complemented strain. We observed that *Hc* lacking Knot2 failed to lyse macrophages to same extent as either wild-type *Hc* or the complemented strain (Figure 3.8B).

Lastly, we explored whether the inability of the *knot2Δ* mutant to fully lyse macrophages was correlated with an intracellular growth defect. As described above for the Knot1 experiment, time points were only collected before the onset of macrophage lysis. *Hc* lacking Knot2 grew well within macrophages, indicating that *KNOT2* is dispensable for intracellular growth (Figure 3.8C).

Taken together these data indicate that *KNOT2* is dispensable for *in vitro* and intracellular growth but required for macrophage lysis.

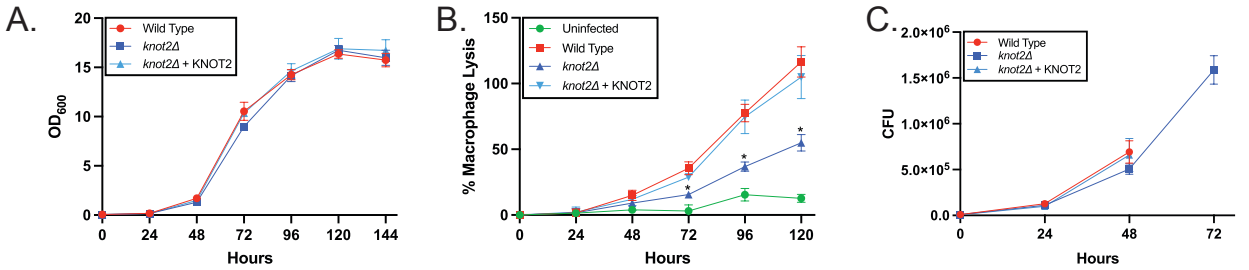

Figure 3.8: *KNOT2* is required for macrophage lysis. (A) *In vitro* growth curve for wild type *Hc* (*ura5Δ* + URA5), *knot2Δ* mutant *Hc* (*ura5Δ*, *knot2Δ* + URA5), *knot2Δ* complemented *Hc* (*ura5Δ*, *knot2Δ* + KNOT2). *Hc* grown in HMM at 37°C, 5% CO_2 for 144 hours. Each strain grown in 100 mL in triplicate. (B) LDH release assay measuring % BMDM lysis over 144 hours. Uninfected BMDMs, or BMDMs infected with wild type *Hc* (*ura5Δ* + URA5), *knot2Δ* mutant *Hc* (*ura5Δ*, *knot2Δ* + URA5), *knot2Δ* complemented *Hc* (*ura5Δ*, *knot2Δ* + KNOT2) at MOI=0.5. All time points relative to time point 0 uninfected cells lysed with 1% Triton in DMEM. (C) Intracellular fungal burden for wild type *Hc* (*ura5Δ* + URA5), *knot2Δ* mutant *Hc* (*ura5Δ*, *knot2Δ* + URA5), *knot2Δ* complemented *Hc* (*ura5Δ*, *knot2Δ* + KNOT2). Time points counted until onset of macrophage lysis.

KNOT3 is required for in vitro growth, macrophage lysis and intracellular growth

To test the role of *KNOT3* during *in vitro* growth, wild type *Hc*, *knot3Δ* mutant *Hc* and *knot3Δ* complemented strain were grown in liquid HMM as described above. We observed that loss of *KNOT3* caused a modest decrease in growth in HMM liquid media (Figure 3.9A). In data not shown, we supplemented the media with uracil and observed the same result, indicating that the growth defect of the *knot3Δ* mutant is not due to an

inability to produce uracil, but is rather due to the absence of *KNOT3*. Further experimentation needs to be done to determine the cause of this phenotype.

Next, we explored the role of Knot3 during infection of BMDMs. BMDMs were either mock-infected, or infected at a MOI of 0.5 with either wild type *Hc*, *knot3Δ* mutant *Hc* or the complemented strain. LDH release assay revealed that Knot3 is required for optimal lysis of macrophages. (Figure 3.9B).

Since the *knot3Δ* mutant has an *in vitro* growth defect, we suspected that the mutant might not grow well inside of macrophages. We infected BMDMs and enumerated the intracellular fungal burden as described above. As expected, we observed that Knot3 is required for intracellular growth of *Hc* within macrophages (Figure 3.9C).

Taken together, these data indicate that *KNOT3* is required for *in vitro* growth, macrophage lysis, and intracellular growth.

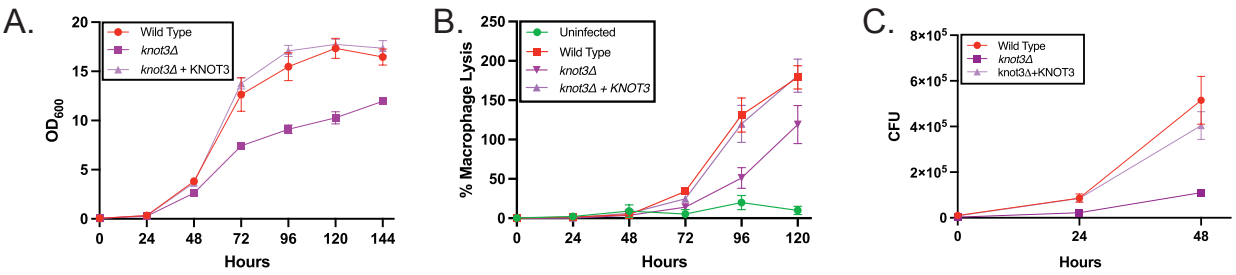

Figure 3.9: *KNOT3* is required for *in vitro* growth, macrophage lysis and intracellular growth. (A) *In vitro* growth curve for wild type *Hc* (*ura5Δ* + URA5), *knot3Δ* mutant *Hc* (*ura5Δ*, *knot3Δ* + URA5), *knot3Δ* complemented *Hc* (*ura5Δ*, *knot3Δ* + KNOT3). *Hc* grown in HMM at 37°C, 5% CO_2 for 144 hours. Each strain was grown in 100 mL in triplicate. (B) LDH release assay measuring % BMDM lysis over 144 hours. Uninfected BMDMs, or BMDMs infected with wild type *Hc* (*ura5Δ* + URA5), *knot3Δ* mutant *Hc* (*ura5Δ*, *knot3Δ* + URA5), *knot3Δ* complemented *Hc* (*ura5Δ*, *knot3Δ* + KNOT3) at MOI=0.5. (C) Intracellular fungal burden for wild type *Hc* (*ura5Δ* + URA5), *knot3Δ* mutant *Hc* (*ura5Δ*, *knot3Δ* + URA5), *knot3Δ* complemented *Hc* (*ura5Δ*, *knot3Δ* + KNOT3). Time points counted until onset of macrophage lysis.

KNOT4 is required for macrophage lysis and intracellular growth

Finally, the role of *KNOT4 in vitro* growth was tested. Wild type *Hc*, *knot4Δ* mutant *Hc* and *knot4Δ* complemented strain were grown in liquid HMM. At day 0, each strain was set to OD 0.05 in triplicate. All cultures were grown at 37°C and 5% CO_2 in an orbital shaker. We observed that loss of *KNOT4* was dispensable for *in vitro* growth (Figure 3.10A).

Next, we explored role of *KNOT4* during infection of BMDMs. BMDMs were either mock-infected, or infected at a MOI of 0.5 with either wild type *Hc*, *knot4Δ* mutant *Hc* or the complemented strain. LDH release assay revealed that Knot4 is required for optimal lysis of macrophages by *Hc* (Figure 3.10B).

To determine if Knot4 affects intracellular growth, we infected BMDMs and examined intracellular fungal burden as described above. We observed that *Hc* lacking Knot4 does not grow well intracellularly (Figure 3.10C).

Taken together, these data indicate that *KNOT4* is dispensable for *in vitro* growth but required for both macrophage lysis and intracellular growth.

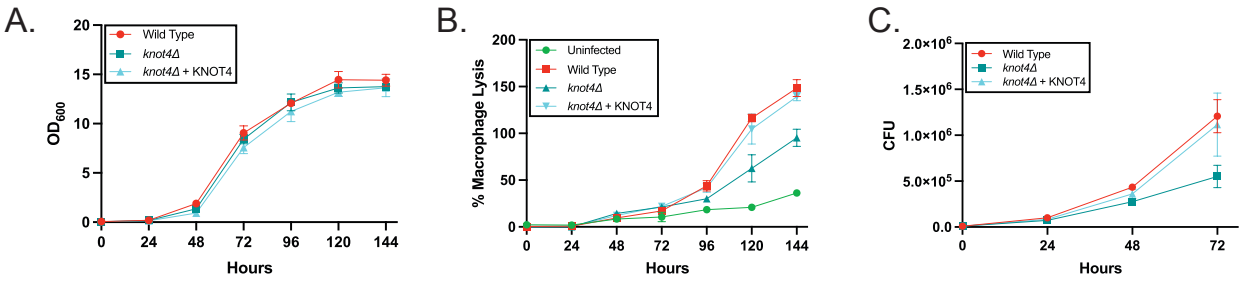

Figure 3.10: *KNOT4* is required for macrophage lysis and intracellular growth. (A) *In vitro* growth curve for wild type *Hc* (*ura5Δ* + URA5), *knot4Δ* mutant *Hc* (*ura5Δ*, *knot4Δ* + URA5), *knot4Δ* complemented *Hc* (*ura5Δ*, *knot4Δ* + KNOT4). *Hc* grown in HMM at 37°C, 5% CO_2 for 144 hours. Each strain grown in 100 mL in triplicate. (B) LDH release assay measuring % BMDM lysis over 144 hours. Uninfected BMDMs, or BMDMs infected with wild type *Hc* (*ura5Δ* + URA5), *knot4Δ* mutant *Hc* (*ura5Δ*, *knot4Δ* + URA5), *knot4Δ* complemented *Hc* (*ura5Δ*, *knot4Δ* + KNOT4) at MOI=0.5. (C) Intracellular fungal burden

for wild type *Hc* (*ura5Δ* + URA5), *knot4Δ* mutant *Hc* (*ura5Δ*, *knot4Δ* + URA5), *knot4Δ* complemented *Hc* (*ura5Δ*, *knot4Δ* + KNOT4). Time points counted until onset of macrophage lysis.

Table 3.2 summarizes the phenotypes observed for *knot1-4* mutants. Importantly, the four knottins fall into 3 phenotypic classes. The first class contains *KNOT1* and *KNOT4* which both are dispensable for *in vitro* growth but are required for macrophage lysis and intracellular growth. The second class contains *KNOT2* which is dispensable for *in vitro* and intracellular growth but is required for macrophage lysis. The third and final class contains *KNOT3* which is required for *in vitro* and intracellular growth as well as macrophage lysis.

Table 3.2: Summary of *knot1-4* phenotypes. ++ Denotes wild type levels of *in vitro* growth in HMM liquid media, BMDM lysis as measured by LDH release assay or intracellular growth as measured CFUs. + Denotes a minor decrease that is statistically significant. +/- Denotes a major decrease as compared to wild type.

Strain	*in vitro* growth	Macrophage lysis	Intracellular growth
WT	++	++	++
knot1	++	+	+
knot2	++	+	++
knot3	+	+	+/-
knot4	++	+	+

Knottin phenotypes are ISR independent

We wondered whether knottins function by inducing cell death through the integrated stress response (ISR) like Cbp1[49]. Briefly, the ISR is an intracellular signaling cascade that is activated after exposure to a variety of stresses, including endoplasmic reticulum (ER) stress and amino acid starvation. ISR induction facilitates return to homeostasis or leads to apoptosis if the stress is unresolved. *Hc* activates the ISR in infected macrophages, as indicated by an increase in eIF2α phosphorylation as well as induction of the transcription factor CHOP and the pseudokinase Tribbles 3 (TRIB3).

To assess whether Knot1-4 affect the ISR, we measured the expression levels of TRIB3 during infection as a proxy for ISR activation. We infected BMDMs with the different knottin mutants and their corresponding complemented strains. RNA was extracted and cDNA was synthesized and subjected to qRT-PCR analysis. Primers used for this analysis are listed in Table 5.2. The overall result was that macrophages infected with the different knottin mutants all induced TRIB3 to a similar extent when compared to macrophages infected with wild-type *Hc*. At time point 0, induction of TRIB3 did not differ from uninfected for all infected samples including wild type. At 24 hours, we observed a statistically significant increase in TRIB3 expression for macrophages infected with either wild-type *Hc* or the knottin mutants and complemented strains. The same result is observed at 48 and 72 hpi. At 96 and 120 hpi, we observed a slightly significant decrease in *TRIB3* induction for macrophages infected with the *knot1Δ* mutant when compared to wild type infected macrophages; however, there is still noticeable induction above uninfected. Overall, we conclude that ISR induction is not dependent on these four knottins, suggesting that they affect other host pathways (Figure 3.11).

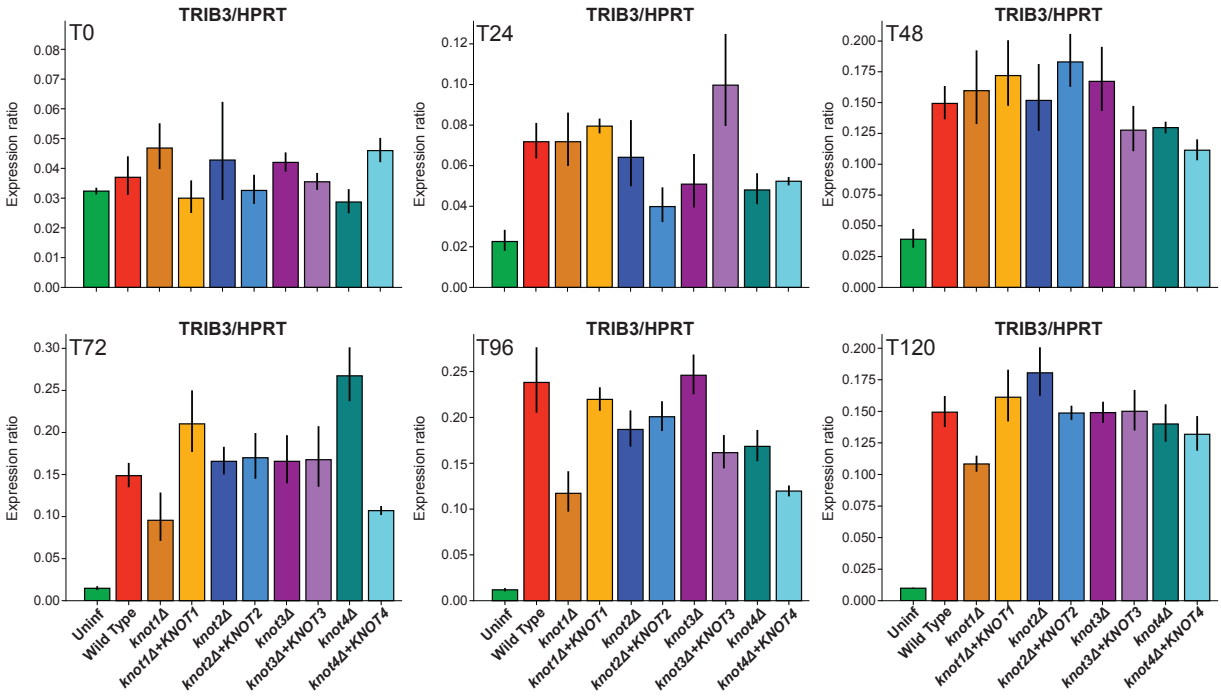

Figure 3.11: Knot1-4 phenotypes are ISR independent. qRT-PCR of TRIB3 expression relative to HPRT as a housekeeping gene. BMDMs were infected at MOI=0.5. RNA was extracted at given time points (0, 24, 48, 72, 96 and 120 hours post infection). Strains used were wild type (*ura5Δ* + URA5), *knot1Δ* (*ura5Δ*, *knot1Δ* + URA5), *knot1Δ* complemented (*ura5Δ*, *knot1Δ* + KNOT1), *knot2Δ* (*ura5Δ*, *knot2Δ* + URA5), *knot2Δ* complemented (*ura5Δ*, *knot2Δ* + KNOT2), *knot3Δ* (*ura5Δ*, *knot3Δ* + URA5), *knot3Δ* complemented (*ura5Δ*, *knot3Δ* + KNOT3), *knot4Δ* (*ura5Δ*, *knot4Δ* + URA5), *knot4Δ* complemented (*ura5Δ*, *knot4Δ* + KNOT4).

Transcriptional profiling of knot4Δ shows a subtle but significant host response

Next, we wondered whether any of the knottin mutants would elicit a distinct host transcriptional response in macrophages when compared to wild-type *Hc.* We did transcriptional profiling of BMDMs infected with wild-type or mutant *Hc* at an MOI=2 and collected infected cells at 48 hours post infection. This scheme allowed us to collect samples right before the onset of macrophage cell death. We extracted RNA from BMDMs and prepared libraries using the Nextera directional library preparation kit.

Prepared libraries were sent for sequencing on the Hiseq4000 at the UCSF Center for Advanced Technology (CAT).

PCA analysis of the RNAseq revealed some interesting findings. Most of the variance in the data was found in the first and second components. The first component contained approximately 50% of the variance and separated the samples based on the state (infected or uninfected) of the macrophages. The second component contained around 15% of the variance and separated samples based on replicate status, which is denoted by circles, triangles, and stars in the PCA. For example, uninfected macrophages shown in green are completely separated from wild-type *Hc*-infected macrophages shown in red. *cbp1Δ*-infected macrophages in black are located closer to the uninfected samples. In contrast, *knot1Δ*-infected macrophages in orange and *knot2Δ* in blue are essentially undistinguishable from wild type at this timepoint and MOI. However, the PCA reveals a subtle but significant difference in the response to *knot4Δ* mutant *Hc* (Figure 3.12).

Looking at significantly changing transcripts that are *knot4Δ* dependent yields a short list of host genes. The simplified heat map (Figure 3.13) shows transcripts that are changing at least 2-fold in the infection with the *knot4Δ* deletion mutant. In red, we show transcripts that are up during infection and in green are transcripts that are down during infection relative to uninfected. Each column is a replicate where each sample was run in triplicate. Each row represents a particular transcript. The *knot4Δ* profile is intermediate between the response to wild-type *Hc* and uninfected/*cbp1Δ* mutant *Hc.* Some of these Knot4-dependent changes include transcripts involved in the immune response like aconitate decarboxylase 1 (Acod1) which is induced during infection with different

pathogens like *Mycobacterium tuberculosis*. Gpr84 is a G-protein coupled receptor which functions as an enhancer for inflammatory signaling in macrophages. Interleukin 1 receptor antagonist (Il1rn) inhibits the activity of Il1α and Il1β, which are cytokines involved in the acute phase of infection and inflammation. More generally this data set may generate hypotheses about how *Hc* causes lysis in the macrophages. (Figure 3.13).

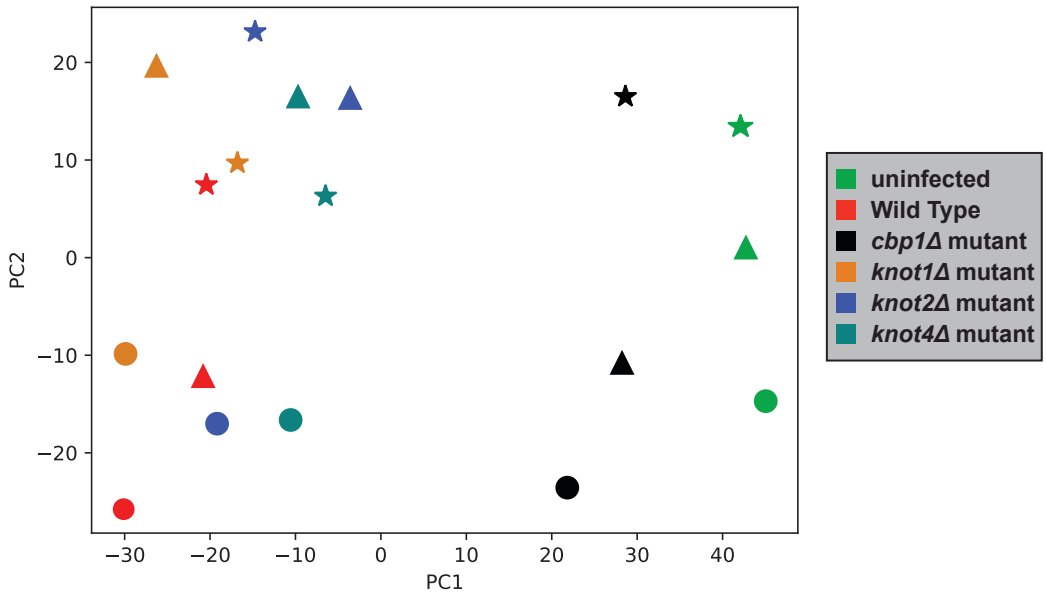

Figure 3.12: PCA of transcriptional profiling of *knot4Δ* shows a subtle host response. The first component contained ~50% of the variance and separated the samples based on the state of the macrophages. The second component contained ~15% of the variance and separated samples based on replicate which are denoted by a circles, triangles, and stars. Uninfected BMDMs are in green, wild type infected (*ura5Δ* + URA5) are in red, *knot1Δ* infected BMDMs are in orange (*ura5Δ*, *knot1Δ* + URA5), *knot2Δ* infected BMDMs are in blue (*ura5Δ*, *knot2Δ* + URA5), *knot4Δ* infected BMDMs are in teal (*ura5Δ*, *knot4Δ* + URA5), and *cbp1Δ* infected BMDMs are in black (*ura5Δ*, *cbp1Δ* + URA5).

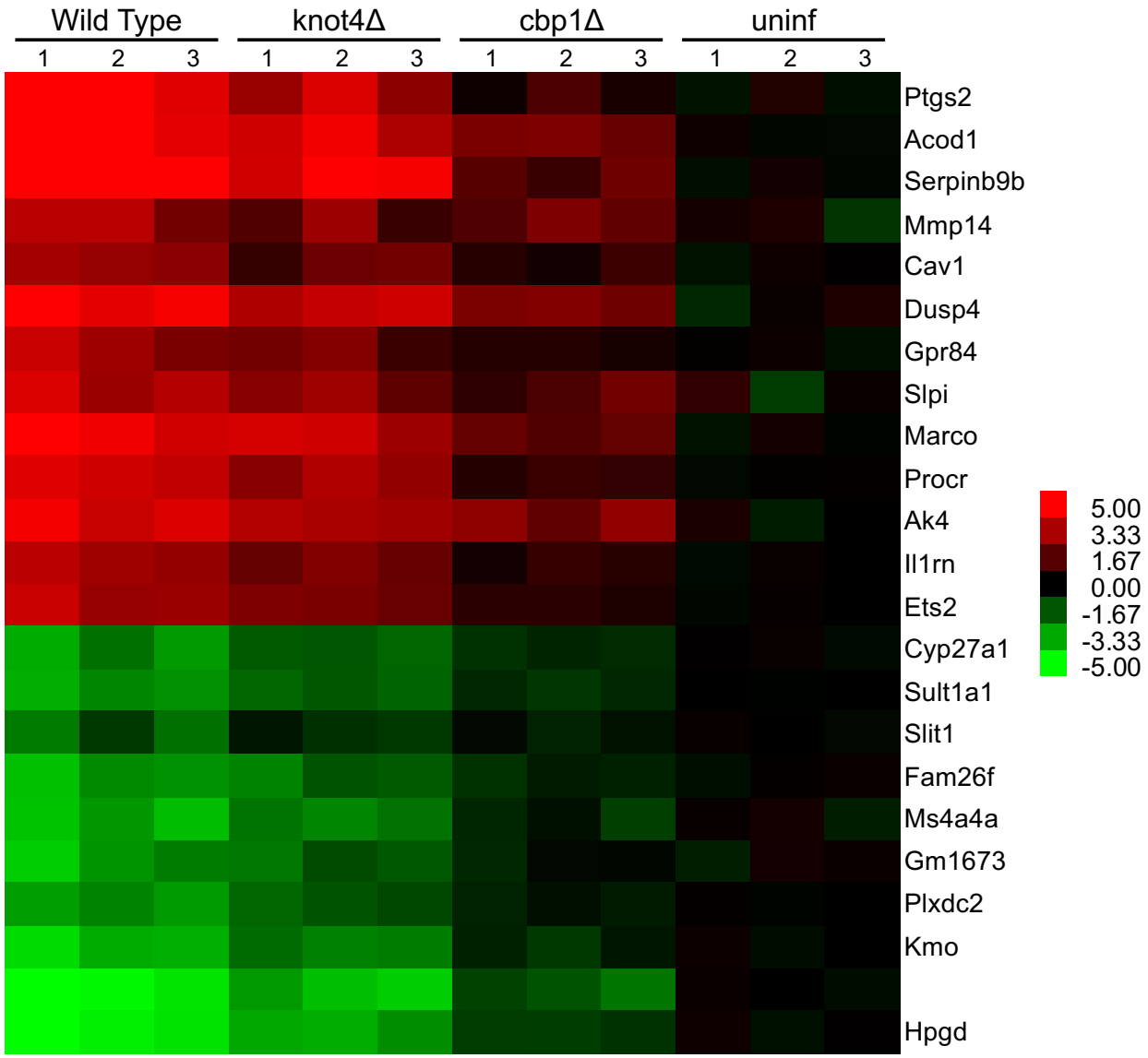

Figure 3.13: Heatmap of differentially expressed transcripts during *Hc* infection. Heatmap of 2-fold significantly changing transcripts in *knot4Δ* mutant infected macrophages. Each sample was run in triplicate. Data is normalized to uninfected number of transcript reads. Upregulated transcripts (red) and downregulated transcripts (green) are presented here.

Discussion and future directions

We explored the role of knottins in *Hc* pathogenesis. We selected four knottins for further characterization and named them *KNOT1-4*. Knot1-4 are highly expressed yeast specific transcripts making them high priority candidates for *Hc* effectors (Figure 3.1).

KNOT1-4 are divided into distinct gene clades. We found orthologs of these knottins within different *Histoplasma* species genomes (G217B, G186AR, H88, H143 and WU24). *KNOT1* is found in clade 12 and across the different *Histoplasma* species we only found one ortholog. Additionally, each ortholog is highly conserved at the protein sequence level. *KNOT4* is found in clade 6 and like *KNOT1* we only found one ortholog in each genome. At the protein sequence level, Knot4 is also highly conserved. Of note, *KNOT4* is the homolog of *C. fulvum AVR9*, the founding member of the knottin Fungi1 family. *KNOT2* is found in clade 9 and unlike *KNOT1* we find paralogs within the different *Histoplasma* species. Specifically, within the G217B genome we found one paralog for *KNOT2* (Knottin_012, Table 2.2). Additionally, the protein sequences are less conserved in this gene clade. *KNOT3* is found in clade 11. *KNOT3* had 6 identified paralogs within the G217B genome (Knottins_001, Knottins_008, Knottins_010, Knottins_016, Knottins_018, and Knottins_021, Table 2.2). The presence of paralogs might indicate some functional redundancy for some of the knottins (Figure 3.2).

We experimentally validated that Knot1-4 are secreted by yeast into culture supernatants and observed the presence of these knottins in the host cytosol by subcellular fractionation of infected macrophages. These data suggest that knottins are secreted by *Hc* yeast in the macrophage phagosome and that they then access the host

cytosol by unknown means. As such, they may be ideally positioned to interact with molecules and pathways in the host cytosol.

We used CRISPR-Cas9 technology to generate targeted deletion mutants of *KNOT1-4* and validated them by PCR (Figure 3.5C) and genome sequencing. Using the mutant and complemented strains, we observed that *KNOT1*, *KNOT2,* and *KNOT4* were all dispensable for *in vitro* growth in HMM. Surprisingly, *Hc* lacking *KNOT3* had a modest growth defect. We speculate that *KNOT3* could be involved in nutrient acquisition. In the future exploring the nature of this growth defect could shed light on the function of *KNOT3*. One could test whether conditioned media or various nutritional supplements could rescue the growth defect of the mutant.

We also determined that *KNOT1*, *KNOT3,* and *KNOT4* are required for macrophage lysis and intracellular growth whereas *KNOT2* was dispensable for intracellular growth. The *KNOT3* result was not surprising since it also has an *in vitro* growth defect. These results place the four knottins into three classes. The first class consists of *KNOT1* and *KNOT4*, the second class consist of *KNOT3* and lastly the third class consists of *KNOT2* (Table 3.2). None of these knottins are required to induce the ISR, indicating that they are not required for induction of that Cbp1-dependent pathway.

Given the large expansion of the knottin family in *Hc*, as well as the presence of multiple paralogs in individual clades, it is surprising that we found phenotypes for mutants lacking individual knottins. In the future it will be interesting to generate various combinations of mutants lacking multiple knottins. Such mutants may have more severe phenotypes. Furthermore, assessing the host transcriptional response at multiple times post-infection and with multiple mutant strains may shed light on knottin function.

Future work will focus on the mechanism of action of individual knottin proteins. As secreted factors, the knottins could acquire nutrients for yeast cells, or they could be interacting with host cell targets to cause disease. It is completely possible that individual knottins might have an unexplored toxic effect on the host. Perhaps solving the protein structures of the individual knottins and/or defining interacting factors will give some insights into potential functions. These experiments are crucial to understanding the role of the knottins during *Hc* infections.

Chapter 4: Knot2 and Knot4 are required for virulence in the mouse model of infection

Introduction

Knot1-4 have phenotypes *in vitro* and in macrophage infections, but as putative virulence factors, it was critical to assess their role in animal infections. Using the standard mouse model of *Hc* infection[47, 49, 59] we explored how loss of individual knottins affects the ability of *Hc* to cause disease *in vivo*.

We wanted to prioritize which knottins to assess in the mouse. Based on the phenotypes observed in Chapter 3 (Table 3.2) we selected two knottins to test *in vivo*. Since *KNOT3* is necessary for *in vitro* growth, we were less interested in testing its role *in vivo*. *KNOT2* was required only for macrophage lysis and was dispensable for intracellular growth, which made it extremely interesting to determine how it affects pathogenesis *in vivo*. Mutants lacking *KNOT1* or *KNOT4* behaved very similarly phenotypically, since each is required for optimal macrophage lysis and intracellular growth. Ultimately, we decided to test the role of Knot4 in the mouse model because of the transcriptional profiling from Chapter 3 (Figure 3.12 and 3.13) which showed a subtle but significant response difference of macrophages to the *knot4Δ* mutant.

knot2Δ and knot4Δ are avirulent in vivo

First, we explored whether loss of *KNOT2* or *KNOT4* affects the virulence of the yeast *in vivo*. C57BL/6 mice were infected intranasally with wild-type, *knot2Δ* or *knot4Δ* mutants, or the complemented strains. A lethal dose of $1x10^6$ *Hc* yeast was used. Mice were monitored for weight loss and disease symptoms (hunching, panting, ears tucked back and/or lack of grooming) over the course of 21 days. Remarkably, both Knot2 (Figure 4.1A) and Knot4 (Figure 4.3A) were required for virulence in the mouse model of infection.

Although mice infected with the corresponding mutants suffer a modest weight loss, they go on to fully recover (Figure 4.1B and 4.3B).

Knot2 and Knot4 affect colonization in vivo

Next, we examined the role of Knot2 and Knot4 in *Hc* colonization of the mouse. C57BL/6 mice were infected intranasally with wild-type, mutant, or complementation strains at a sublethal dose of *Hc* ($3x10^5$ yeast). Surprisingly, *knot4Δ* mutant *Hc* show a moderate decrease in fungal burden in lungs beginning as early as 1-day post-infection (dpi) and persisting through the remainder of the infection (Figure 4.4). Fungal burden is also decreased in the spleen starting at 3 dpi and persisting throughout the infection (Figure 4.4). Given the strength of the virulence defect, it was surprising that fungal burden was only modestly affected. These data suggest that *KNOT4* might influence other factors in addition to growth in vivo.

In the case of *KNOT2*, fungal burden was transiently down at 5 dpi in the lungs but reached wild-type levels by 9 dpi. Fungal burden was comparable to wild-type in the spleen (Figure 4.2). Again, given the strength of the virulence defect, it is surprising that fungal burden is essentially the same as wild-type *Hc*. Future experiments will assess whether critical elements of the host response, such as cytokine production and host inflammation, are altered in mutant vs. wild-type infection. If so, these data would suggest that the knottins are influencing the host immune response to infection.

A.

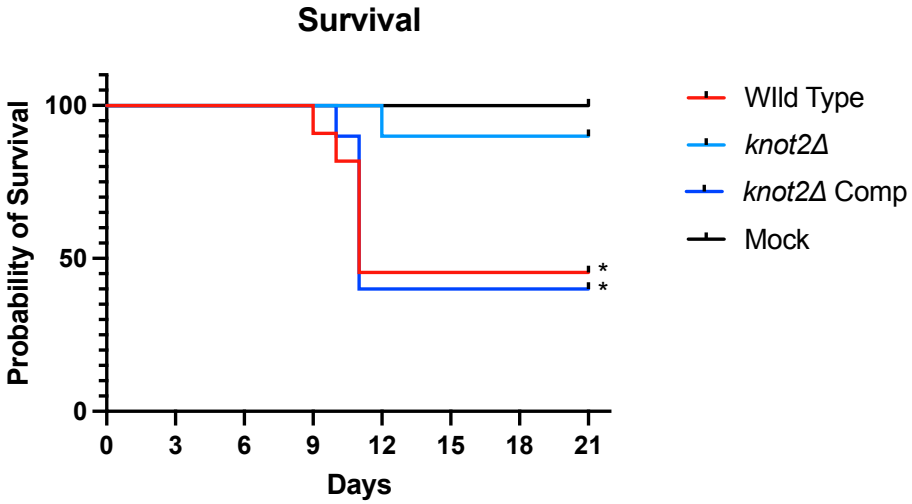

B.

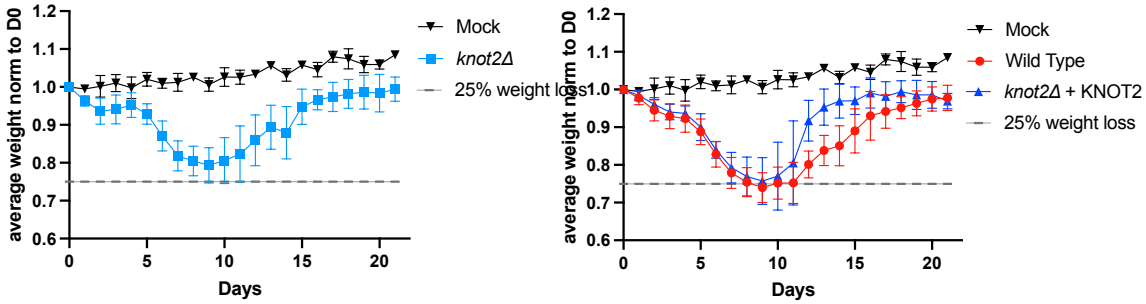

Figure 4.1: Kaplan-Meier survival curve shows *knot2Δ* is avirulent in the mouse model of infection. (A) Loss of *KNOT2* showed a significant decrease in virulence. Approximately ~60-70% Wild type (n=11) or complement (n=10) infection mice succumbed to the infection. Mice infected with *knot2Δ* mutant *Hc* almost all survived (N=10) as shown by the Kaplan Meyer survival curve. Mock (N=3) all survived. p-value<0.05 one-way ANOVA test. (B) Weight of mice normalized to day 0. *knot2Δ* mutant *Hc* (light blue) infected mice lost weight but never reached 25% weight loss (grey line). Mock infected (black) are included as a comparison. Wild type *Hc* (red) infected mice or *knot2Δ* complement (dark blue) infected mice decreased in weight earlier and reached 25% weight loss.

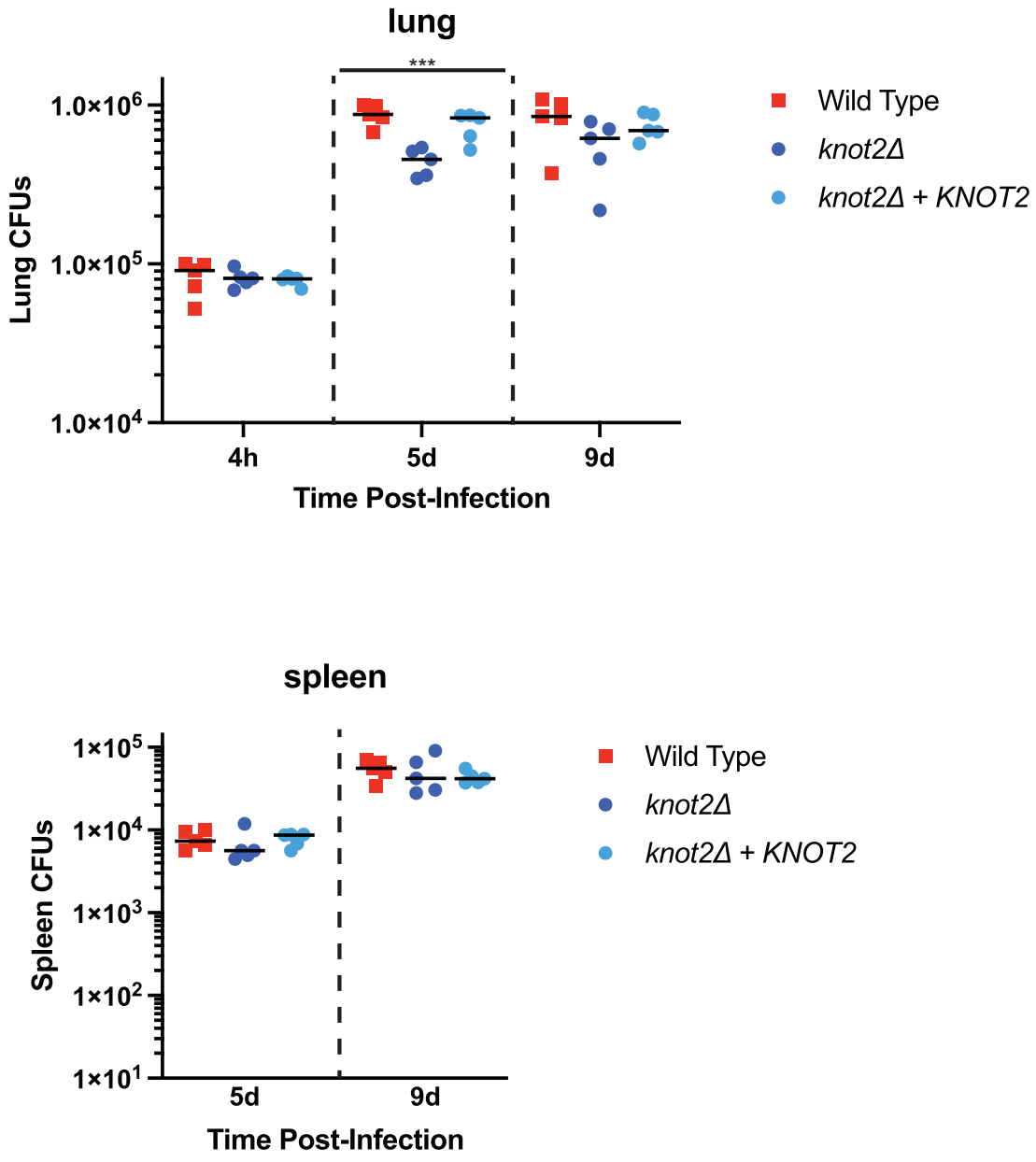

Figure 4.2: Fungal burden in mouse lungs shows moderate decrease for *knot2Δ* mutant *Hc*. Sublethal dose of *Hc* was administered to anesthetized mice. Five mice are infected per genotype per time point. One-way ANOVA test showed significant change in fungal burden only in the lungs at 5 dpi. Strains tested included wild type (*ura5Δ* + URA5), *knot2Δ* (*ura5Δ*, *knot2Δ* + URA5), *knot2Δ* complemented strain (*ura5Δ*, *knot2Δ* + KNOT2). p-value<0.005. Top panel is CFUs for lungs and bottom panel is CFUs for spleens.

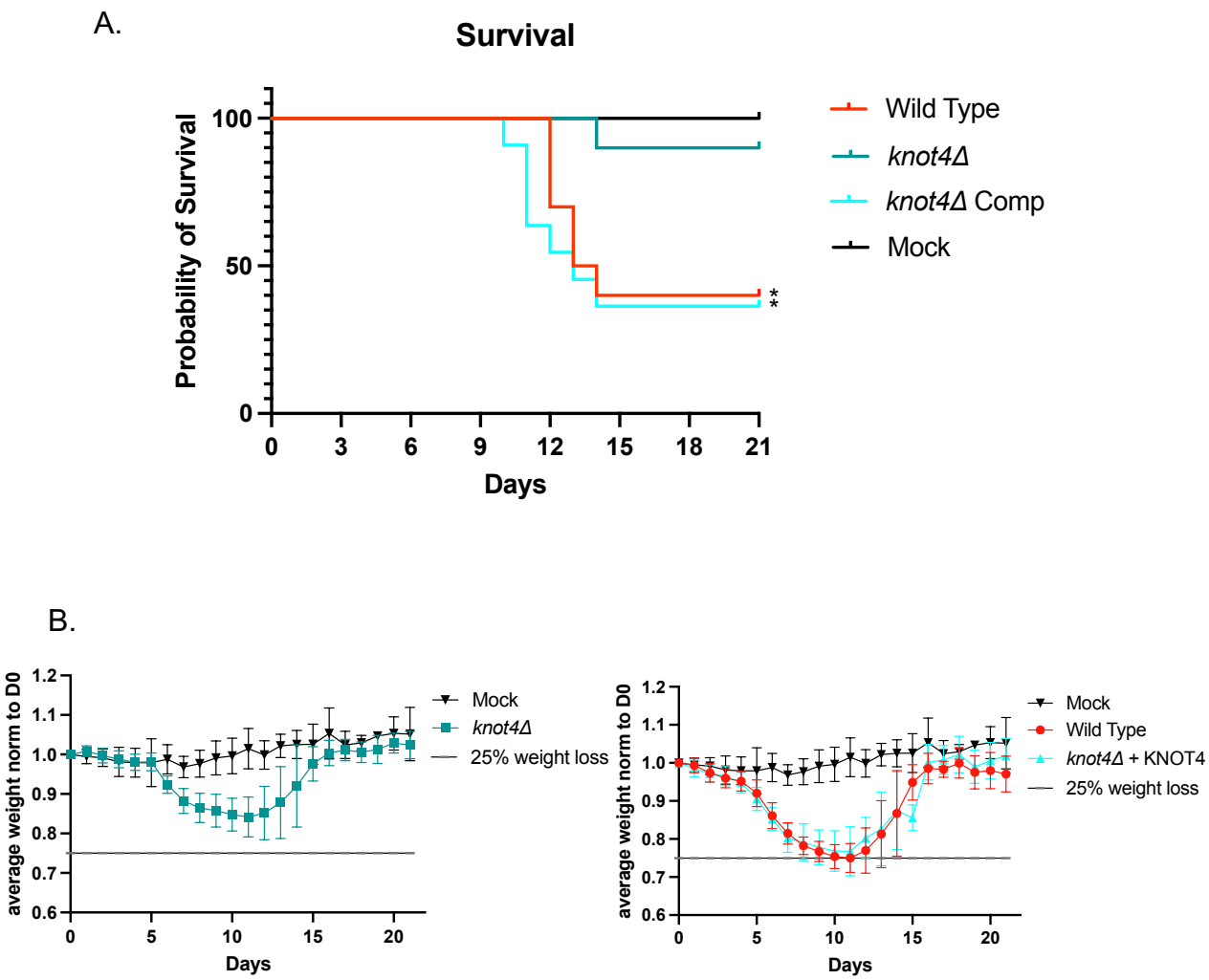

Figure 4.3: Kaplan-Meier survival curve shows *knot4Δ* is avirulent in the mouse model of infection. (A) Loss of *KNOT4* showed a significant decrease in virulence. Approximately ~65-75% of wild type (n=10) or complement (n=11) infection mice succumbed to the infection. Mice infected with *knot4Δ* mutant *Hc* almost all survived (N=10) as shown by the Kaplan Meyer survival curve. Mock (N=3) all survived. p-value<0.05 one-way ANOVA test. (B) Weight of mice normalized to day 0. *Knot4Δ* mutant *Hc* (teal) infected mice lost weight but never reached 25% weight loss (grey line). Mock infected (black) are included as a comparison. Wild type (red) or complement (cyan) infected mice lost more weight and reached the 25% weight loss threshold.

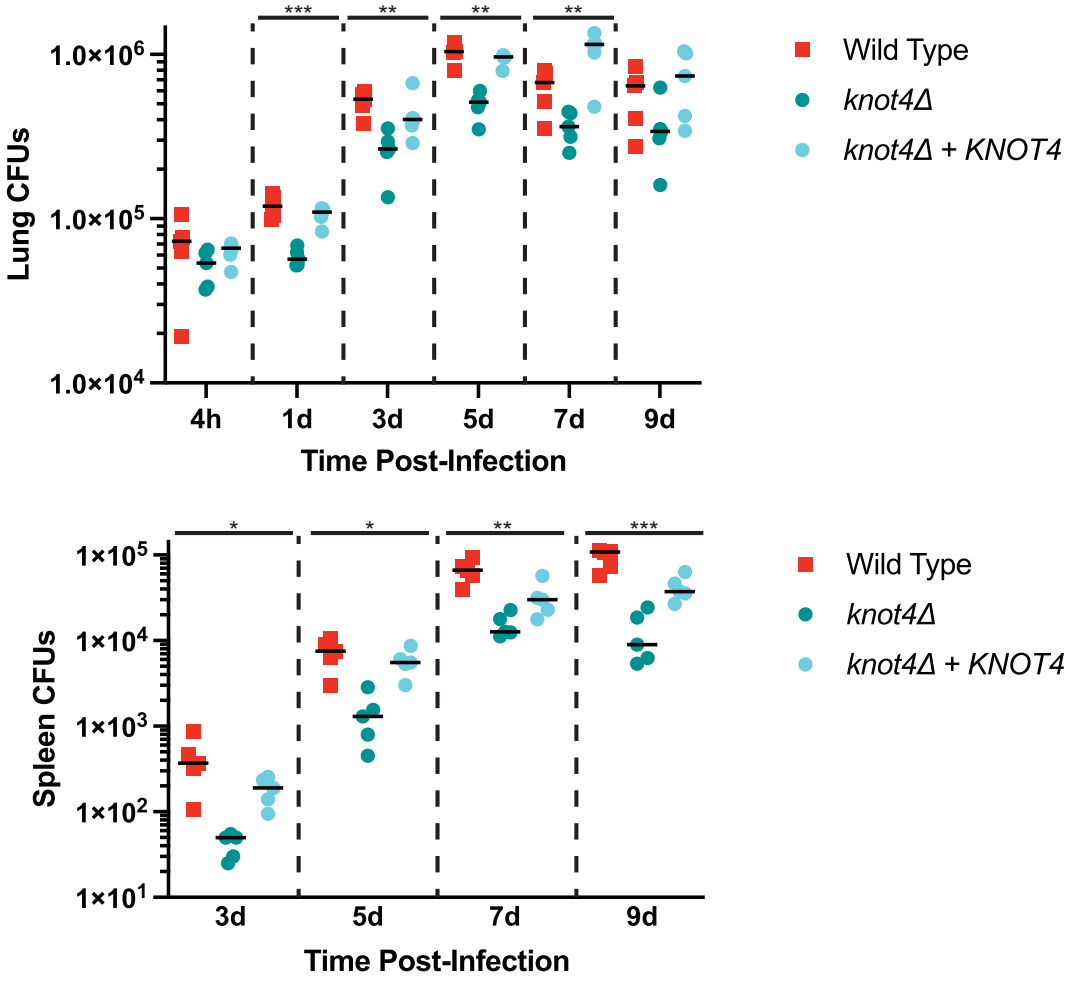

Figure 4.4: Fungal burden in mouse lungs and spleens shows moderate decrease for *knot4Δ* mutant *Hc*. Sublethal dose of *Hc* was administered to anesthetized mice. Five mice are infected per genotype per time point. One-way ANOVA test showed significant change in fungal burden. Strains tested included wild type (*ura5Δ* + URA5), *knot4Δ* (*ura5Δ*, *knot4Δ* + URA5), *knot4Δ* complemented strain (*ura5Δ*, *knot4Δ* + KNOT4). p-value<0.05. Top panel is CFUs for lungs and bottom panel is CFUs for spleens.

Discussion and future directions

Our experiments indicate that knottins are key effectors that play important roles in *Hc* virulence. We observed that mutants lacking either Knot2 or Knot4 were avirulent in mice. Importantly, the weight loss of the mice indicated that they were experiencing symptoms of illness when infected with the mutants, but these mice were able to recover, indicating that the host was able to control infection. Interestingly, we observed that Knot2 was largely dispensable for fungal burden, except for a transient decrease in fungal burden in the lung at 5 dpi. Future experiments will include a high-density time course of fungal burden in the mouse to fully capture the kinetics of fungal growth *in vivo*. In the case of Knot4, the mutant displayed reproducibly lower fungal burden at all time points examined, in both lung and spleen. However, although there is a statistically significant decrease in fungal burden compared to wild-type infection, the mutant is still present at relatively high levels. This suggests that Knot4 may affect other processes *in vivo* in addition to fungal growth, thus accounting for the virulence defect. Future experiments will query the host immune response and histopathology during infection with mutant vs. wild-type *Hc*. These experiments may reveal a role for knottins in manipulating the host response to *Hc*. Ultimately, a full understanding of knottin biology in *Hc* pathogenesis will include generating an atlas of host responses to a variety of knottin mutants. What is clear is that these intriguing effector proteins play key roles in *Hc* infection *in vivo*.

Materials and Methods

Concentrating Hc culture supernatants:

Hc yeast are grown in HMM at 37°C, 5% CO_2 in an orbital shaker until they reach stationary phase. 10-mL of culture are spun down at 2500rpm for 5 minutes at RT. Supernatant is carefully removed from pellet. Supernatant is passed through 0.22 μm filter to sterilize. Sterile culture supernatants are concentrated using MilliporeSigma™ Amicon™ Centrifugal filter units with a 3 kDa molecular weight cut off (MWCO) to ensure we save as many small proteins as possible. Spin conditions are as stated in manufacturer manual. Culture supernatants are concentrated down to ~100uL. They are snap frozen and stored at -80°C until further use.

Fractionation of Hc-infected macrophage lysates

BMDMs ($2.0x10^7$ cells) were plated on 15-cm TC-treated plates and infected with different *Hc* strains (MOI = 5). At 24 hours post infection, cells were gently collected by scraping without washing. Cells were spun down at 2500 rpm for 5 min to pellet. The cell pellet was resuspended in 500 µL of D-PBS (Ca^{2+} Mg^{2+} free) and transferred to a 1.5 mL eppendorf tube and spun at 1000 rpm for 2 min to wash cells. 300µL of homogenization buffer (20mM HEPES pH 7.4, 150mM KCl, 2mM EDTA, cOmplete Mini Protease Inhibitor Cocktail tablet-Roche) was used to suspend cell pellet. Unfractionated sample was resuspended in homogenization buffer containing 1% TritonX-100. The remaining cell lysate (the fractionated sample) was passed through a 27-gauge needle making sure to avoid bubbles. This ensures only the plasma membrane is ruptured and not any internal membranous organelles. The lysate is then spun at 3000rpm for 5 minutes to pellet *Hc* cells and macrophage nuclei and remove them. The lysate was then

centrifuging twice at 3000 rpm with removal of 275 µL and 250 µL respectively to avoid contamination of the lysate with *Hc*. Finally, 225 µL was placed in ultracentrifuge tubes (Beckman Coulter 349622), carefully weighed, and loaded into a Beckman Coulter Fixed Angle Rotor TLA100.3. The samples were spun at 45,000 rpm for 2 hours in a TL-100 tabletop ultracentrifuge. In the end, 175µL of supernatant is transferred into a separate 1.5 mL low binding tube which represents the cytosolic fraction. To avoid cross contamination, remaining cytosolic fraction is discarded. The pellet is resuspended in 225 µL of homogenization buffer with 1% TritonX-100 which represents the membrane fraction. All samples were flash frozen in liquid nitrogen and stored at -80°C.

SDS-PAGE Protein gel and western blot analysis

Protein samples were mixed with 4X Protein Loading Buffer (Li-COR 926–31097) and 1:20 DTT (1M DTT) and denatured at 95°C for 5 minutes. Proteins were separated by SDS-PAGE on NOVEX-NuPAGE 4–12% BIS-TRIS gels with MES Running Buffer and Precision Plus Dual Xtra Protein Standards (Bio-Rad161-0377) were used to estimate the molecular weight of proteins. For Western blots, the SDS-PAGE separated proteins were transferred to nitrocellulose membranes. Non-specific binding to the membrane was blocked with Odyssey PBS Blocking Buffer (Fisher Scientific NC9877369) and probed with the antibodies listed below. Blots were imaged on an Odyssey CLx and analyzed using ImageStudio2.1 (Li-COR). The following primary antibodies were used: monoclonal mouse anti-FLAG M2 (Millipore Sigma F3165), custom generated Rabbit anti-Cbp1 (Rb83), mouse anti-alpha-tubulin (Novus biological DM1A), and Rabbit anti-calnexin (abcam 22595).

Generation of Hc strains

H. capsulatum strain G217B *ura5Δ* (WU15) was a kind gift from the lab of William Goldman (University of North Carolina, Chapel Hill). For all studies in this paper, "wild type" refers to G217B *ura5Δ* transformed with a *URA5*-containing episomal vector (pLH211). The knottin deletion mutants were all generated from the G217B *ura5Δ* parental strain transformed with an episomal plasmid which contains a bi-directional H2Ab promoter driving Cas9 and two sgRNA cassettes targeting the sequences on both sides of the G217B knottin genes (*KNOT1-4*). Single colony isolates were selected for screening by PCR to identify edited genomic sites. Single colony isolates were repeated isolated and screened until wild type copy of the gene of interest was not detected by PCR. Plasmid containing the Cas9 (pBJ219) was lost from the mutants by growing the *Hc* yeast in HMM containing exogenous uracil and then screening through colonies for plasmid loss. The purified mutant *Hc* were finally transformed with either the *URA5*-containing episomal plasmid (pLH211) and a URA5-containing complementation vector. All tagged knottin strains used in this study were C-terminally tagged with 3XFLAG under their native promoters and introduced into *Hc* G217B *ura5Δ*. For all *Hc* transformations, approximately 100 ng of PacI-linearized DNA was electroporated into appropriate parental strains (G217B *ura5Δ*, G217B *ura5Δ*, *knot1Δ*, G217B *ura5Δ, knot2Δ*, G217B *ura5Δ knot3Δ* , or G217B *ura5Δ knot4Δ*) as previously described. The plasmid pLH211 was used as a vector control. All transformants were selected on HMM agarose plates.

DNA isolation and PCR:

Using the Qiagen Gentra Puregene Yeast/Bact. Kit, two-day late log *Hc* cultures were used for DNA isolation as per manufacturer protocol. Takara PrimeSTAR GXL DNA polymerase was used to amplify genomic regions. Primers that were used in reactions are listed in Table 5.1. Standard 25uL reactions were run on Thermal cycler with cycling parameters as follows: 98°C for 10s, followed by 35 cycles of 60°C for 15s, 68°C for 120s. PCR products were run on a 1% agarose gel and imaged on a Biorad machine.

Table 5.1: List of primers used to screen *knot1-4* CRISPR deletion mutants.

Primer Name	Sequence
KNOT1 external forward	GTGCTAGCACATGAGTGGGGAT
KNOT1 external reverse	TCCCCCCACCAGAGCTTCG
KNOT1 internal forward	GGAGAGTAGAAAACATAAACCTCATTCATAACTCAGAGA
KNOT1 internal reverse	AACATACACCAGCCTTACTACCACTTGC
KNOT2 external forward	GTACTTCAGATGGTCAGGACGGCT
KNOT2 external reverse	AGATAGATAGGCAGGTAGGCAGGC
KNOT2 internal forward	TCGCTCTTTGTGTTGCTACCAATGATGTC
KNOT2 internal reverse	CCAGAGGTTGAGCATATTATGTCTTTCCTCTGG
KNOT3 external forward	ATCGTTATTCTAGAATGAGGGCCTGAACCAT
KNOT3 external reverse	AATTTAAATCACATCCACCCATTACAAATTTTCGATAT GCTGGC
KNOT3 internal forward	GGTGTTCTGTTCATCACGTGATCATAAAGGA
KNOT3 internal reverse	TGAATAAACCGAATATCCAATAAGTTAGGCGCTG
KNOT4 external forward	TTAAGCAATGGTACGCCCGCT
KNOT4 external reverse	CTGCTAGGAATTATGTCAAGAACTGCATG
KNOT4 internal forward	TCAGTGTTATTGCTTATGAAAACTTGGTGAGTAGTATCT
KNOT4 internal reverse	TCCATGAGGATAACAGTGATTTATTCGATGGGATAA

RNA isolation

For RNA isolation from *Hc* yeast cells, 10mL of two-day late log *Hc* yeast culture was pelleted and resuspended in 1 mL of QIAzol (Qiagen). Sample in QIAzol were transferred to 2mL screw cap tubes with ~1/3 of the volume filled with zirconia beads. Samples were bead-beaten in a Mini-BeadBeater-96 (BioSpec 1001) for 2 minutes to lyse cells. After bead beating, chloroform (200 μL) was added and vigorously vortexed for 15 seconds. Lysates were centrifuged at 12,000xg for 20 minutes at 4°C. The aqueous phase was used for RNA purification. For RNA isolation from cultured cells, BMDMs were seeded ($1x10^6$ cells per well of a 6-well plate) and infected in triplicate. Triplicate wells of infected macrophages were lysed in 1mL total of QIAzol (Qiagen). Again, the aqueous phase was saved for RNA purification. Total RNA was isolated from the aqueous phase using Econo-spin columns (Epoch Life Science) and then subjected to on-column PureLink DNase (Invitrogen) digestion. Total RNA was eluted into nuclease free water.

qRT-PCR

To generate cDNA for qRT-PCR analysis, 2-4 µg total RNA was reverse transcribed using Maxima Reverse Transcriptase (Thermo Scientific), an oligo-dT primer, and pdN9 primers following manufacturer's instructions. Quantitative PCR was performed on 1:10 to 1:50 dilutions of cDNA template using FastStart SYBR Green MasterMix with Rox (Roche). Reactions were run on an Mx3000P machine (Stratagene) and analyzed using MxPro software (Stratagene). Cycling parameters were as follows: 95°C for 10 min, followed by 40 cycles of 95°C (30 s), 55°C (60 s), and 72°C (30 s), followed by dissociation curve analysis. Abundances of TRIB3 were normalized to HPRT levels. *KNOT1*, *KNOT2*,

KNOT3 and *KNOT4* levels were normalized to *Hc* GAPDH levels. Primer sequences are listed in Table 5.2.

Table 5.2: List of primers used for qRT-PCR analysis for expression in *Hc* and TRIB3 expression in macrophages.

Primer Name	Sequence
Hc_KNOT1 qPCR forward	CGACTACGGAGAGTAGAAAACATAAACCTCATTC
Hc_KNOT1 qPCR reverse	CTGTTGGATTCTCTCAGATGGTAGTAAATGG
Hc_KNOT2 qPCR forward	CACTATTTCTCCTTTACGTCTCTGGGC
Hc_KNOT2 qPCR reverse	TCCTCATGTTTTCTGGTAAGCCATGGTAGT
Hc_KNOT3 qPCR forward	GAAGCTTATTATTTTATATATTGAGATTATTTTCTTAA TGCAGCAAGTATTAG
Hc_KNOT3 qPCR reverse	CAATGAATAAACCGAATATCCAATAAGTTAGGCG
Hc_KNOT4 qPCR forward	CAGGTTTAAATTTTATTATTTTCAGTGTTATTGCTTAT GAAAACTTG
Hc_KNOT4 qPCR reverse	CTTTCTTACTTTGAGCTGTCATGACAGTG
Hc_GAPDH	AGACCCACTATGCtgCCTACA
Hc_GAPDH	GGGTCGTATGTTTTCTCGT
mTrib3 qPCR forward	TGCAGGAAGAAACCGTTGGAG
mTrib3 qPCR reverse	CTCAGGCTCATCTCTCACTCG
mHPRT qPCR forward	AGGTTGCAAGCTTGCTGGT
mHPRT qPCR reverse	TGAAGTACTCATTATAGTCAAGGGCA

mRNA isolation and RNAseq library preparation

Equal amounts of total RNA (1µg total) were used for each sample. RNA quality was assessed using RNA 6000 Nano Bioanalyzer chip (Agilent Technologies). mRNA was purified using polyA selection with Oligo-dT Dynabeads (Thermo Fisher Scientific) as described in the manufacturer's protocol. Ribosomal RNA depletion was confirmed using RNA 6000 Nano Bioanalyzer chip. Libraries were prepared using the NEBNext Ultra II Directional RNA Library Prep Kit (New England Biolabs). NEBNext Multiplex Oligos for

Illumina sequencing platform (New England Biolabs) were used to uniquely barcoded individual libraries. Average fragment size was between 300-500bp. For efficient library sequencing presence of excess adapter was determined by running libraries on a High Sensitivity DNA Bioanalyzer chip (Agilent Technologies). Concentration of individual libraries was determined using the High Sensitivity DNA Qubit assay (Thermo Fisher Scientific). A total of 5 ng per library was pooled and sequenced at UCSF Center for Advanced Technology (CAT) on an Illumina HiSeq 4000 sequencer.

BMDM culture conditions

Bone marrow derived macrophages (BMDMs) were isolated from the tibias and femurs of 6-8 week-old C57BL/6J (Jackson Laboratories stock, No. 000664) mice. Mice were euthanized via CO_2 narcosis and cervical dislocation as approved under UCSF Institutional Animal Care and Use Committee protocol # AN197403-01. Cells were differentiated in BMM (bone marrow derived macrophage media) which consists of Dulbecco's Modified Eagle Medium, D-MEM High Glucose (UCSF Cell Culture Facility), 20% Fetal Bovine Serum (Atlanta Cat #: S11150, Lot #: D18043 or Corning Cat #: 35010CV, Lot #: 05820001), 10% v/v CMG supernatant (the source of CSF-1), 2 mM glutamine (UCSF Cell Culture Facility), 110 µg/mL sodium pyruvate (UCSF Cell Culture Facility), 100X penicillin and 100X streptomycin (UCSF Cell Culture Facility). Undifferentiated monocytes were plated in BMM for 7 days at 37°C and 5% CO_2. Adherent cells were then scraped and frozen down in 40% FBS and 10% DMSO and stored in liquid nitrogen for future use.

Macrophage infections

Macrophage infections with G217B *Hc* strains were performed as described previously[47-49, 60]. Briefly, the day before infection, macrophages were seeded in tissue culture-treated dishes in triplicate. On the day of infection, yeast cells from logarithmic-phase *Hc* cultures (OD_{600} = 4–7) were collected, resuspended in D-PBS (PBS that is free of Ca^{2+} and Mg^{2+}, UCSF Cell Culture Facility) sonicated for 3 seconds on setting 2 using a Fisher Scientific Sonic Dismembrator Model 100, and counted using a hemacytometer at 40X magnification. Depending on the multiplicity of infection (MOI), the appropriate number of yeast cells was then added to the macrophages in BMM. After a 2-hour phagocytosis period, the macrophages were washed once with D-PBS to remove any extracellular yeast and fresh BMM media was added. For infections lasting longer than 2 days, fresh BMM media was added to the cells at approximately 48 hours post infection.

Lactate dehydrogenase release assay

To quantify macrophage lysis, BMDMs were seeded (7.5×10^4 cells per well of a 48-well plate) and infected in triplicate as described above. At the indicated time points, the amount of LDH in the supernatant was measured as described previously[61, 62]. BMDM lysis was calculated as the percentage of total LDH from supernatant of wells with uninfected macrophages lysed in 1% Triton X-100 at the time of infection. Due to continued replication of BMDMs over the course of the experiment, the total LDH at later time points can be greater than the total LDH from the initial time point, resulting in an apparent lysis that is greater than 100%.

Intracellular replication

BMDMs were seeded ($7.5x10^4$ cells per well of a 48-well plate) and infected in triplicate as described above. At the indicated timepoints, culture supernatants were removed and 500 µl of ddH_2O was added. Cells were incubated at 37°C for 15 min and then mechanically lysed by vigorously pipetting. The lysate was collected, sonicated to disperse any clumps, and counted on a hemocytometer at 40X magnification. Appropriate dilutions were performed and *Hc* is plated on HMM agarose. Plates are incubated at 37°C with 5% CO_2 for 12–14 days after which time CFUs were enumerated. To prevent any extracellular replication from confounding the results, intracellular replication was not monitored after the onset of macrophage lysis.

In vitro Histoplasma capsulatum growth

Two-day, late-log *Hc* cultures were used to inoculate 100 mL of HMM medium to a starting OD_{600} = 0.05 in triplicate. Cultures were incubated in an orbital shaker at 37°C with 5% CO_2 for 144 hours. At each timepoint, 1 mL of each culture flask was removed, vigorously vortexed for 30 seconds, diluted to be within the linear range, and analyzed to determine their OD_{600} on spectrophotometer.

Mouse infections

Eight-to-twelve week-old female C57BL/6 mice (Jackson Laboratory stock, No. 000664) were anesthetized with isoflurane and infected intranasally with wild type *Hc* (G217B *ura5Δ* + URA5), the *knot2Δ* mutant (*knot2Δ* + URA5), the complemented stain (*ura5Δ, knot2Δ* + KNOT2), the *kno4Δ* mutant (*ura5Δ, knot4Δ* + URA5) or the complemented stain (*ura5Δ, knot4Δ* + KNOT4). The inoculum was prepared by collecting mid-logarithmic phase (OD_{600} = 4–7) yeast cultures, washing once with D-PBS

(Ca^{2+}, Mg^{2+} free), sonicating for 3 seconds on setting 2 using a Fisher Scientific Sonic Dismembrator Model 100, counting with a hemacytometer, and diluting with D-PBS so the final inoculum was approximately 30 µL. To monitor survival, animals were infected intranasally with 1.0×10^6 yeast per mouse. Infected mice were monitored daily for symptoms of disease, including weight loss, hunching, panting, and lack of grooming. For survival curve analysis, mice were euthanized after they exhibited 3 days of sustained weight loss greater than 25% of their maximum weight in addition to one other symptom. To confirm correct inoculum and proper intranasal infection, the inoculum itself and the 4 hr post-infection lungs for 2 mice per condition were harvested and homogenized in D-PBS and plated on brain heart infusion (BHI) agar plates supplemented with 10% sheep's blood. CFU's were enumerated after 10–12 days of growth at 30°C. To monitor fungal burden, animals were infected intranasally with 3.0×10^5 yeast per mouse. At every time point, 5 mice per genotype were euthanized and lungs and spleens were harvest at appropriate time points. Organs were homogenized in D-PBS and plated on brain heart infusion (BHI) agar plates supplemented with 10% sheep's blood at appropriate time points. CFU's were enumerated after 10–12 days of growth at 30°C.

KNOTTIN Finder

Knottin 6-cysteine motif tends to be in a single open reading frame (ORF). Using this information, we wrote a novel and naïve algorithm called KNOTTIN Finder to detect knottins in the *Hc* genome. Steps are listed in Figure 2.4. We selected genes with ORFS ≤750 nucleotides (i.e. predicted small proteins) and with no overlap to annotated transcripts with mature CDS longer than 750 nucleotides.

Knottin expansion across fungi

KNOTTIN Finder hits were aligned to Hidden Markov Model (HMM) from Gilmore, S. et. al. (2015)[30]. All putative Knottin hits were run against 623 fungal genomes found in the ENSEMBL database as well as *Cladosporium fulvum*, *Sphaeroforma arctica,* and *Dictyostelium discoideum* genomes from GenBank. All hits were grouped taxonomically based on Gcd10p phylogeny and determined to be in 15 distinct gene clades. Final figure only showing representative species, 66 in total. Final array tree branch lengths are not to scale.

Protein alignments

Different clades were determined as described above. Individual probcons (Probabilistic Consistency-based Multiple Alignment of Amino Acid Sequences)[63] alignments of knottins clades were run to identify paralogs within the different *Hc* species (G217B, G186AR, WU24, H88, H143 and Tmu).

Reference:

1. Alto, N.M. and K. Orth, *Subversion of cell signaling by pathogens.* Cold Spring Harb Perspect Biol, 2012. **4**(9): p. a006114.
2. Kellermann, M., F. Scharte, and M. Hensel, *Manipulation of Host Cell Organelles by Intracellular Pathogens.* Int J Mol Sci, 2021. **22**(12).
3. Omotade, T.O. and C.R. Roy, *Manipulation of Host Cell Organelles by Intracellular Pathogens.* Microbiol Spectr, 2019. **7**(2).
4. Hakimi, M.A. and A. Bougdour, *Toxoplasma's ways of manipulating the host transcriptome via secreted effectors.* Curr Opin Microbiol, 2015. **26**: p. 24-31.
5. Augenstreich, J. and V. Briken, *Host Cell Targets of Released Lipid and Secreted Protein Effectors of Mycobacterium tuberculosis.* Front Cell Infect Microbiol, 2020. **10**: p. 595029.
6. Mittal, E., et al., *Mycobacterium tuberculosis Type VII Secretion System Effectors Differentially Impact the ESCRT Endomembrane Damage Response.* mBio, 2018. **9**(6).
7. Chandra, P., S.J. Grigsby, and J.A. Philips, *Immune evasion and provocation by Mycobacterium tuberculosis.* Nat Rev Microbiol, 2022. **20**(12): p. 750-766.
8. Hamon, M., H. Bierne, and P. Cossart, *Listeria monocytogenes: a multifaceted model.* Nat Rev Microbiol, 2006. **4**(6): p. 423-34.
9. Peron-Cane, C., et al., *Fluorescent secreted bacterial effectors reveal active intravacuolar proliferation of Listeria monocytogenes in epithelial cells.* PLoS Pathog, 2020. **16**(10): p. e1009001.

10. Chauhan, D. and S.R. Shames, *Pathogenicity and Virulence of Legionella: Intracellular replication and host response.* Virulence, 2021. **12**(1): p. 1122-1144.
11. Fontana, M.F., et al., *Secreted bacterial effectors that inhibit host protein synthesis are critical for induction of the innate immune response to virulent Legionella pneumophila.* PLoS Pathog, 2011. **7**(2): p. e1001289.
12. Henkel, J.S., M.R. Baldwin, and J.T. Barbieri, *Toxins from bacteria.* EXS, 2010. **100**: p. 1-29.
13. Green, E.R. and J. Mecsas, *Bacterial Secretion Systems: An Overview.* Microbiol Spectr, 2016. **4**(1).
14. Lanver, D., et al., *Ustilago maydis effectors and their impact on virulence.* Nat Rev Microbiol, 2017. **15**(7): p. 409-421.
15. Kim, K.T., et al., *Evolution of the Genes Encoding Effector Candidates Within Multiple Pathotypes of Magnaporthe oryzae.* Front Microbiol, 2019. **10**: p. 2575.
16. de Wit, P.J., et al., *Correction: The Genomes of the Fungal Plant Pathogens Cladosporium fulvum and Dothistroma septosporum Reveal Adaptation to Different Hosts and Lifestyles But Also Signatures of Common Ancestry.* PLoS Genet, 2015. **11**(12): p. e1005775.
17. de Wit, P.J., *Cladosporium fulvum Effectors: Weapons in the Arms Race with Tomato.* Annu Rev Phytopathol, 2016. **54**: p. 1-23.
18. Moyes, D.L., et al., *Candidalysin is a fungal peptide toxin critical for mucosal infection.* Nature, 2016. **532**(7597): p. 64-8.
19. Avery, S.V., et al., *The fungal threat to global food security.* Fungal Biol, 2019. **123**(8): p. 555-557.

20. Case, N.T., et al., *The future of fungi: threats and opportunities.* G3 (Bethesda), 2022. **12**(11).

21. Fisher, M.C., et al., *Threats Posed by the Fungal Kingdom to Humans, Wildlife, and Agriculture.* mBio, 2020. **11**(3).

22. Pradhan, A., et al., *Fungal effectors, the double edge sword of phytopathogens.* Curr Genet, 2021. **67**(1): p. 27-40.

23. Buitrago, M.J. and M.T. Martin-Gomez, *Timely Diagnosis of Histoplasmosis in Non-endemic Countries: A Laboratory Challenge.* Front Microbiol, 2020. **11**: p. 467.

24. Arauz, A.B. and P. Papineni, *Histoplasmosis.* Infect Dis Clin North Am, 2021. **35**(2): p. 471-491.

25. Woods, J.P., *Revisiting old friends: Developments in understanding Histoplasma capsulatum pathogenesis.* J Microbiol, 2016. **54**(3): p. 265-76.

26. Kauffman, C.A., *Histoplasmosis: a clinical and laboratory update.* Clin Microbiol Rev, 2007. **20**(1): p. 115-32.

27. Lockhart, S.R., et al., *Endemic and Other Dimorphic Mycoses in The Americas.* J Fungi (Basel), 2021. **7**(2).

28. Maiga, A.W., et al., *Mapping Histoplasma capsulatum Exposure, United States.* Emerg Infect Dis, 2018. **24**(10): p. 1835-1839.

29. Conant, N.F., *Cultural Study of the Life-Cycle of Histoplasma capsulatum Darling 1906.* J Bacteriol, 1941. **41**(5): p. 563-79.

30. Gilmore, S.A., et al., *Genome-Wide Reprogramming of Transcript Architecture by Temperature Specifies the Developmental States of the Human Pathogen Histoplasma.* PLoS Genet, 2015. **11**(7): p. e1005395.

31. Mittal, J., et al., *Histoplasma Capsulatum: Mechanisms for Pathogenesis.* Curr Top Microbiol Immunol, 2019. **422**: p. 157-191.

32. Deepe, G.S., Jr., R.S. Gibbons, and A.G. Smulian, *Histoplasma capsulatum manifests preferential invasion of phagocytic subpopulations in murine lungs.* J Leukoc Biol, 2008. **84**(3): p. 669-78.

33. Howard, D.H., *Intracellular Growth of Histoplasma Capsulatum.* J Bacteriol, 1965. **89**(2): p. 518-23.

34. Howard, D.H., *Intracellular Behavior of Histoplasma Capsulatum.* J Bacteriol, 1964. **87**(1): p. 33-8.

35. Gildea, L.A., et al., *Human dendritic cell activity against Histoplasma capsulatum is mediated via phagolysosomal fusion.* Infect Immun, 2005. **73**(10): p. 6803-11.

36. Newman, S.L., et al., *Human macrophages do not require phagosome acidification to mediate fungistatic/fungicidal activity against Histoplasma capsulatum.* J Immunol, 2006. **176**(3): p. 1806-13.

37. Shen, Q. and C.A. Rappleye, *Differentiation of the fungus Histoplasma capsulatum into a pathogen of phagocytes.* Curr Opin Microbiol, 2017. **40**: p. 1-7.

38. Beyhan, S., et al., *A temperature-responsive network links cell shape and virulence traits in a primary fungal pathogen.* PLoS Biol, 2013. **11**(7): p. e1001614.

39. Nguyen, V.Q. and A. Sil, *Temperature-induced switch to the pathogenic yeast form of Histoplasma capsulatum requires Ryp1, a conserved transcriptional regulator.* Proc Natl Acad Sci U S A, 2008. **105**(12): p. 4880-5.

40. Rappleye, C.A. and W.E. Goldman, *Defining virulence genes in the dimorphic fungi.* Annu Rev Microbiol, 2006. **60**: p. 281-303.

41. Garfoot, A.L. and C.A. Rappleye, *Histoplasma capsulatum surmounts obstacles to intracellular pathogenesis.* FEBS J, 2016. **283**(4): p. 619-33.

42. Holbrook, E.D., et al., *Redundant catalases detoxify phagocyte reactive oxygen and facilitate Histoplasma capsulatum pathogenesis.* Infect Immun, 2013. **81**(7): p. 2334-46.

43. Youseff, B.H., et al., *Extracellular superoxide dismutase protects Histoplasma yeast cells from host-derived oxidative stress.* PLoS Pathog, 2012. **8**(5): p. e1002713.

44. Howard, D.H., et al., *Hydroxamate siderophores of Histoplasma capsulatum.* Infect Immun, 2000. **68**(4): p. 2338-43.

45. Dade, J., et al., *HcZrt2, a zinc responsive gene, is indispensable for the survival of Histoplasma capsulatum in vivo.* Med Mycol, 2016. **54**(8): p. 865-75.

46. Batanghari, J.W. and W.E. Goldman, *Calcium dependence and binding in cultures of Histoplasma capsulatum.* Infect Immun, 1997. **65**(12): p. 5257-61.

47. Azimova, D., et al., *Cbp1, a fungal virulence factor under positive selection, forms an effector complex that drives macrophage lysis.* PLoS Pathog, 2022. **18**(6): p. e1010417.

48. Isaac, D.T., et al., *Macrophage cell death and transcriptional response are actively triggered by the fungal virulence factor Cbp1 during H. capsulatum infection.* Mol Microbiol, 2015. **98**(5): p. 910-929.

49. English, B.C., et al., *The transcription factor CHOP, an effector of the integrated stress response, is required for host sensitivity to the fungal intracellular pathogen Histoplasma capsulatum.* PLoS Pathog, 2017. **13**(9): p. e1006589.

50. Ron, D., *Translational control in the endoplasmic reticulum stress response.* J Clin Invest, 2002. **110**(10): p. 1383-8.

51. Karine de Guillen, C.L., Pascale Tsan, Philippe Barthe, Benjamin Petre, Natalya Saveleva, Nicolas Rouhier, Sébastien Duplessis, André Padilla & Arnaud Hecker, *Structural genomics applied to the rust fungus Melampsora larici-populina reveals two candidate effector proteins adopting cystine knot and NTF2-like protein folds.* 2019.

52. Jérôme Gracy, D.L.-N., 3 Jean-Christophe Gelly,4 Quentin Kaas,5 Annie Heitz,1,2 and Laurent Chiche, *KNOTTIN: the knottin or inhibitor cystine knot scaffold in 2007.* 2007.

53. Ackerman, S.E., et al., *Cystine-knot peptides: emerging tools for cancer imaging and therapy.* Expert Rev Proteomics, 2014. **11**(5): p. 561-72.

54. Lee, S.Y. and R. MacKinnon, *A membrane-access mechanism of ion channel inhibition by voltage sensor toxins from spider venom.* Nature, 2004. **430**(6996): p. 232-5.

55. Huang, Y.H., et al., *The biological activity of the prototypic cyclotide kalata b1 is modulated by the formation of multimeric pores.* J Biol Chem, 2009. **284**(31): p. 20699-707.

56. Loo, S.N., et al., *Identification and Characterization of Roseltide, a Knottin-type Neutrophil Elastase Inhibitor Derived from Hibiscus sabdariffa.* Scientific Reports, 2016. **6**.

57. Kall, L., A. Krogh, and E.L. Sonnhammer, *A combined transmembrane topology and signal peptide prediction method.* J Mol Biol, 2004. **338**(5): p. 1027-36.

58. Kall, L., A. Krogh, and E.L. Sonnhammer, *Advantages of combined transmembrane topology and signal peptide prediction--the Phobius web server.* Nucleic Acids Res, 2007. **35**(Web Server issue): p. W429-32.

59. Cohen, A., et al., *Genome-scale CRISPR screening reveals that C3aR signaling is critical for rapid capture of fungi by macrophages.* PLoS Pathog, 2022. **18**(9): p. e1010237.

60. Hwang, L.H., et al., *Histoplasma requires SID1, a member of an iron-regulated siderophore gene cluster, for host colonization.* PLoS Pathog, 2008. **4**(4): p. e1000044.

61. Isaac, D.T., et al., *The 3-hydroxy-methylglutaryl coenzyme A lyase HCL1 is required for macrophage colonization by human fungal pathogen Histoplasma capsulatum.* Infect Immun, 2013. **81**(2): p. 411-20.

62. Decker, T. and M.L. Lohmann-Matthes, *A quick and simple method for the quantitation of lactate dehydrogenase release in measurements of cellular*

cytotoxicity and tumor necrosis factor (TNF) activity. J Immunol Methods, 1988. **115**(1): p. 61-9.

63. Do, C.B., et al., *ProbCons: Probabilistic consistency-based multiple sequence alignment.* Genome Res, 2005. **15**(2): p. 330-40.

Publishing Agreement

It is the policy of the University to encourage open access and broad distribution of all theses, dissertations, and manuscripts. The Graduate Division will facilitate the distribution of UCSF theses, dissertations, and manuscripts to the UCSF Library for open access and distribution. UCSF will make such theses, dissertations, and manuscripts accessible to the public and will take reasonable steps to preserve these works in perpetuity.

I hereby grant the non-exclusive, perpetual right to The Regents of the University of California to reproduce, publicly display, distribute, preserve, and publish copies of my thesis, dissertation, or manuscript in any form or media, now existing or later derived, including access online for teaching, research, and public service purposes.

DocuSigned by:
Rosa Rodriguez
203C158D29124B4...
Author Signature

3/16/2023
Date